Nanodevice development for network-based biocomputation: Scaling up and performance optimization

Surendiran, Pradheebha

2023

Document Version:
Publisher's PDF, also known as Version of record

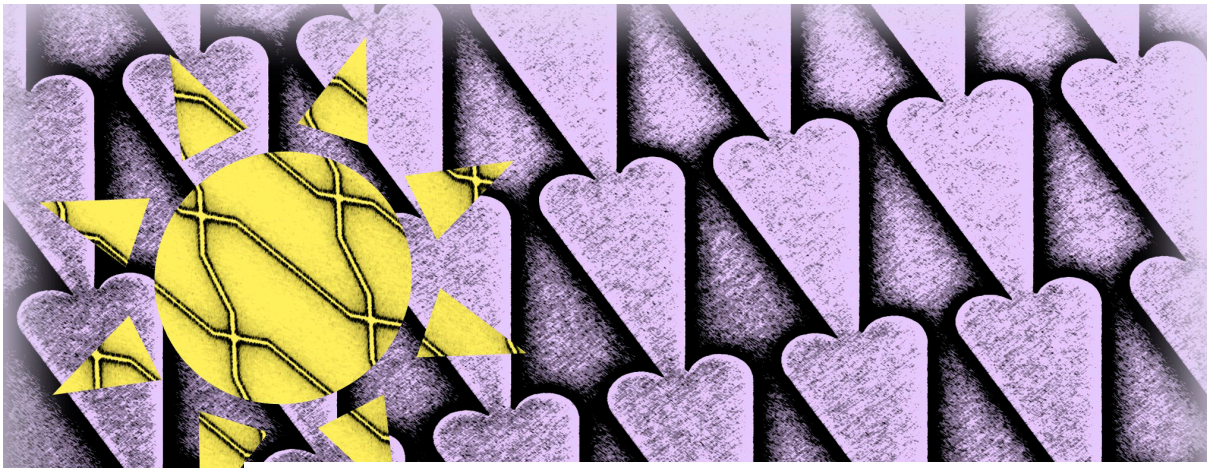

Nanodevice development for network-based biocomputation

Scaling up and performance optimization

PRADHEEBHA SURENDIRAN
DEPARTMENT OF PHYSICS | FACULTY OF ENGINEERING | LUND UNIVERSITY

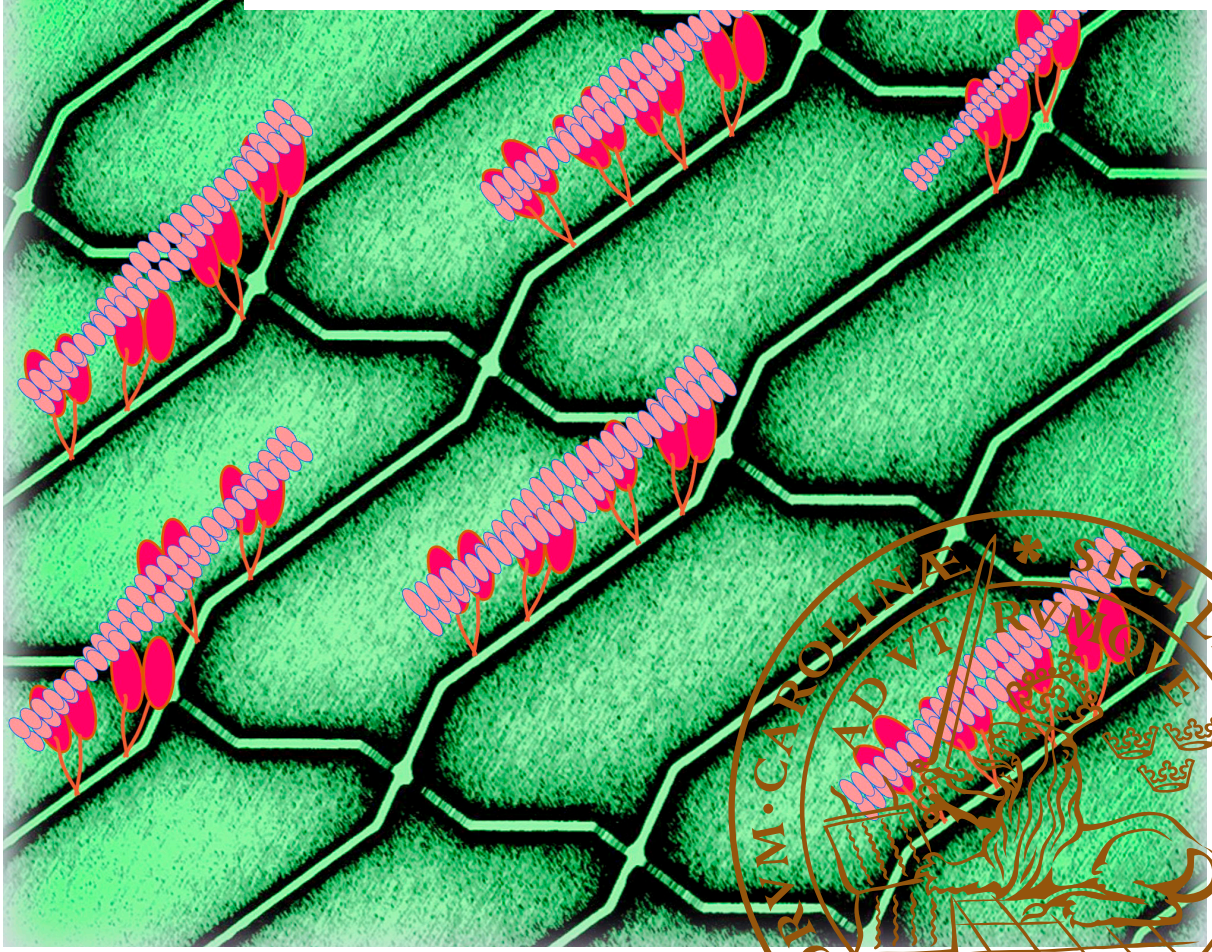

Nanodevice development for network-based biocomputation: Scaling up and performance optimization

Nanodevice development for network-based biocomputation:

Scaling up and performance optimization

Pradheebha Surendiran

LUND
UNIVERSITY

DOCTORAL DISSERTATION

Doctoral dissertation for the degree of Doctor of Philosophy (PhD) at the Faculty of Engineering at Lund University to be publicly defended on Friday, November 10th, 2023, at 9.15 in Rydbergsalen, Department of Physics, Sölvegatan 14.

Faculty Opponent
Prof. Dr. Michel Calame
EMPA, Switzerland

Organization: LUND UNIVERSITY

Document name: Doctoral dissertation **Date of issue:** 2023-11-10

Author(s): Pradheebha Surendiran **Sponsoring organization:**

Title and subtitle: Nanodevice development for network-based biocomputation: Scaling up and performance optimization

Abstract:
The combinatorial nature of several practically important mathematical problems, including non-deterministic polynomial-time (NP) complete problems, makes it necessary to search through a very large solution space. Solving these problems using electronic computers is limited due to the sequential exploration of all possible solutions that can result in exponential time and high energy. This motivates the need for parallel computing approaches where multiple solutions are explored simultaneously in an energy-efficient manner. Network-based biocomputation (NBC) is an alternate energy-efficient parallel computing technique where problem instances encoded into nanofabricated networks are explored by molecular motor-propelled cytoskeletal filaments to solve the encoded problem instances. Traffic-regulating geometries, such as split and pass junctions, control molecular motors' movement. In orders of magnitude, NBC was demonstrated to be more energy efficient than conventional computers in the proof-of-concept solving of the subset sum problem (SSP), an NP-complete problem.

Some of the important technical advances that were identified to scale up NBC into a competitive technology include (i) the prolonged operation of NBC devices for device performance standardization, (ii) the development of new and effective algorithms to solve different and larger instances of NP-complete problems; and (iii) reduction of the pass-junction error rates. To address the longevity issues, crucial factors such as resist utilized, time required for plasma treatment, and silanization time associated with fabrication and surface modification that enabled prolonged movement of molecular motors in these nanodevices were identified. The optimization of nanodevices for biocompatibility and improved device performance necessary for scaling up NBC is presented herein. With these optimizations, the function of motors was prolonged from <20 min to >60 min.

The solution of two distinct NP-complete problems, namely Exact Cover and Satisfiability, presented in this dissertation demonstrated the capability of NBC beyond SSP. The advancement in solving 5-set instances of Exact Cover and 3-SAT comprising three variables and five clauses has been showcased through the utilization of actin-myosin-based devices. These problems were converted into summation problems that construct the NBC network and further applied to develop algorithms to address diverse combinatorial problems. The problem instances solved in this context were four times larger than the proof-of-concept device with a solution space of eight.

High error rates caused by pass junctions are identified as a major limitation for upscaling NBC. Two different error propagation strategies have been presented: 1) 2D junction geometry optimization and 2) development of 3D junctions. Experiments conducted on various junction designs with different critical parameters to optimize 2D geometry led to the optimized junction having less than 1% error rate compared to the current 2-4% error rate. To completely mitigate error rates, preliminary results of the development of 3D junctions in the form of tunnels and bridges using two-photon polymerization have also been elucidated. The conclusion deliberates on some key technological requirements imperative for NBC scale-up and enumerates plausible solutions to meet these requirements.

Key words: biocomputation, fabrication, NP-complete, molecular motors, motility assay

Language: English **ISSN and key title**:

ISBN: 978-91-8039-811-4 (print) 978-91-8039-812-1 (electronic)

Recipient's notes **Number of pages**: 71

Price **Security classification**

Signature Date 2023-09-28

Nanodevice development for network-based biocomputation:

Scaling up and performance optimization

Pradheebha Surendiran

LUND
UNIVERSITY

Front cover photo by Pradheebha Surendiran. They are enhanced SEM images of the fabricated nanodevices

Back cover photo by Ivan unskov

Faculty of Engineering

Department of Physics, Solid State Physics

ISBN 978-91-8039-811-4 (print)

ISBN 978-91-8039-812-1 (electronic)

Printed in Sweden by Media-Tryck, Lund University

Lund 2023

To my parents, who bestowed their wings upon me to soar

Table of Contents

Abstract

The combinatorial nature of several practically important mathematical problems, including non-deterministic polynomial-time (NP) complete problems, makes it necessary to search through a very large solution space. Solving these problems using electronic computers is limited due to the sequential exploration of all possible solutions that can result in exponential time and high energy consumption. This motivates the need for parallel computing approaches where multiple solutions are explored simultaneously in an energy-efficient manner. Network-based biocomputation (NBC) is an alternate energy-efficient parallel computing technique where problem instances encoded into nanofabricated networks are explored by molecular motor-propelled cytoskeletal filaments to solve the encoded problem instances. Traffic-regulating geometries, such as split and pass junctions, control molecular motors' movement. In orders of magnitude, NBC was demonstrated to be more energy efficient than conventional computers in the proof-of-concept solving of the subset sum problem (SSP), an NP-complete problem.

Some of the important technical advances that were identified to scale up NBC into a competitive technology include (i) the prolonged operation of NBC devices for device performance standardization, (ii) the development of new and effective algorithms to solve multiple and larger instances of NP-complete problems; and (iii) reduction of the pass-junction error rates. To address the longevity issues, crucial factors such as resist utilized, time required for plasma treatment, and silanization time associated with fabrication and surface modification that enabled prolonged movement of molecular motors in these nanodevices were identified. The optimization of nanodevices for biocompatibility and improved device performance necessary for scaling up NBC is presented herein. With these optimizations, the function of motors in the nanodevices was prolonged from <20 min to >60 min.

The solution of two distinct NP-complete problems, namely Exact Cover and Satisfiability (3-SAT), presented in this thesis demonstrated the capability of NBC beyond SSP. The advancement in solving 5-set instances of Exact Cover and 3-SAT comprising three variables and five clauses has been showcased through the utilization of actin-myosin-based devices. These problems were converted into summation problems that construct the NBC network and further applied to develop algorithms to address diverse combinatorial problems. The problem instances solved in this context were four times larger than the proof-of-concept SSP device with a solution space of eight.

High error rates caused by pass junctions are identified as a major limitation for upscaling NBC. Two different error propagation strategies have been presented: 1) 2D junction geometry optimization and 2) development of 3D junctions. Experiments conducted on various junction designs with different critical parameters to optimize 2D geometry led to the optimized junction having less than

1% error rate compared to the current 2-4% error rate. To completely mitigate error rates, preliminary results of the development of 3D junctions in the form of tunnels and bridges using two-photon polymerization have also been elucidated. The conclusion deliberates on some key technological requirements imperative for NBC scale-up and enumerates plausible solutions to meet these requirements.

Popular Science Summary

In the field of mathematics and computer science, there are many complex mathematical problems that hold significant implications for solving real-world applications. For instance, let us delve into the Exact Cover problem that appears naturally in logistics planning and resource allocation. Imagine that you have a bunch of different tasks you need to accomplish, and you want to find the best way to do them without any overlaps. Each task can require different resources or elements, and your goal is to figure out how to select tasks in a manner that uses each resource exactly once. This problem arises in many areas, like scheduling resources or solving puzzles like Sudoku. It is all about finding the right combination of pieces to make everything fit just right!

Let us consider a real-world application of Exact Cover: choosing the right aircraft for a flight depends on factors like destination, flight duration, and passenger count. Solving this problem becomes incredibly challenging as the number of factors grows very large, and the existing algorithms require looking at all possible solutions. This kind of situation is what makes the exact cover problem a non-deterministic polynomial-time (NP-complete) problem. NP-complete problems are like puzzles that become resource-intensive in terms of energy and time consumption to solve as they get bigger. Although you might be able to solve small instances of the exact cover problem relatively easily, an increase in the number of tasks and resources corresponds to increase in the time and energy required for effective problem-solving.

Due to the abovementioned limitations, electronic computers require increased resources to solve these problems as they work in a sequential manner using a single CPU. It is practically impossible to check all possible combinations of resources efficiently. To overcome these challenges, there is a need for energy-efficient parallel computing approaches. Some of the well-known alternative computing strategies are DNA computing and quantum computing. These approaches aim to leverage the unique properties of DNA molecules or quantum systems to tackle complex mathematical problems more efficiently due to the parallel approach and lower energy costs than conventional electronic computers. However, they suffer from limitations such as the requirement of impractically large amounts of DNA and decoherence in quantum entanglement.

A third alternative computing strategy known as "network-based biocomputation (NBC)" harnessing molecular motors as computing agents has been developed. Molecular motors are fascinating tiny machines that exist inside our bodies and other living organisms. They play a crucial role in many biological processes, such as muscle movement, cell division, and transportation within cells. Think of molecular motors as tiny workers that can convert chemical energy into mechanical motion. Just like a motor in a car converts fuel into the spinning motion of its wheels,

molecular motors convert chemical energy into movement on a microscopic scale. These molecular motors are made up of proteins that have specific shapes and structures. They have parts that can bind to other molecules and can change their shape when interacting with energy-rich molecules called Adenosine triphosphate (ATP). When the molecular motor encounters ATP, it grabs onto it and undergoes a shape change, which causes it to move in a particular direction. This process repeats, and each step adds up, allowing the motor to move along a track or exert force on other molecules. We are harnessing this process in the movement of molecular motors within the nanodevice developed for NBC. A significant benefit of these biomolecules is their abundant presence in nature and availability in substantial quantities. Another important advantage is the inherent high energy efficiency of the molecular motors.

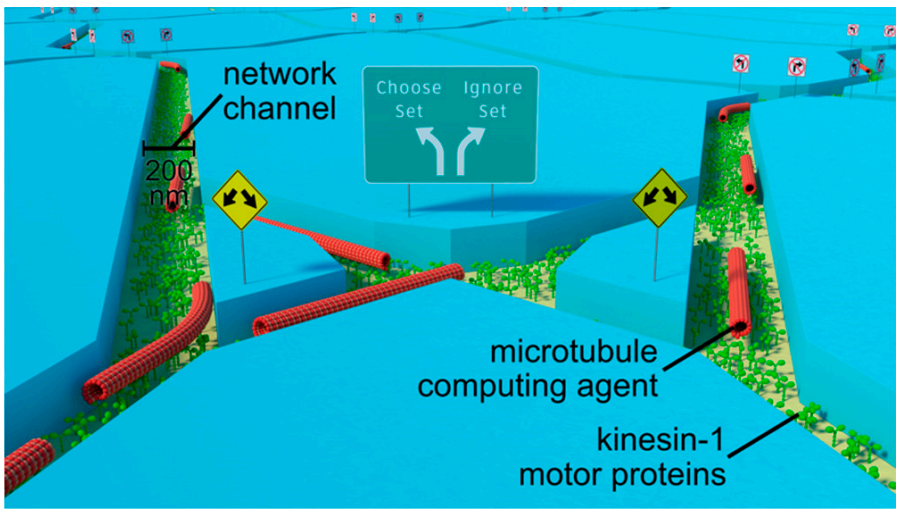

Figure: Schematic rendition of a biocomputation device showing computing agents (red) exploring possible paths inside a network with traffic rules. Each path represents a different calculation. Figure taken from[1] Copyright (2022) ACS Nanoscience Au

NBC operates through two steps: (1) The physical structure of the mathematical problem is crafted to resemble a deliberately constructed maze/network, which is subsequently nanofabricated onto silicon chips. (2) The graphical network is subsequently navigated by molecular motors to carry out the computation by exploring all possible paths, corresponding to the solution space. To comprehend the creation of the graphical network, envision a network of connected roads. The structuring of these network of connected roads is designed with specific criteria to represent the targeted mathematical problem where agents need to obey some traffic

rules. Each pathway within this network corresponds to a distinct calculation and can lead to diverse destinations, representing all different, possible solutions to the problem instance. In NBC, this process takes place on a microscopic scale, where the networks and agents are nanosized. Each problem instance necessitates the formation of a unique maze tailored to its calculations and solutions.

Like road networks with junctions, the problem instance's graphical network also features crossings called junctions. These junctions enforce specific traffic rules to ensure the cytoskeletal filaments reach their intended destinations. Junctions are designed so that the agents do not take U-turns or diversions, where traffic must only proceed straight, following its initial path. However, it is an error when the agents deviate from their intended paths and move in different directions. This type of error has been recognized as a significant impediment to the NBC scale-up.

This thesis focuses on improving nanodevice performance created through network fabrication. This dissertation not only discusses the crucial parameters related to the fabrication and surface functionalization of these nanodevices but also envisages to improve the effectiveness and durability of agents within the nanodevices. Using optimized nanodevices, solving two instances of the Exact Cover problem is has been successfully demonstrated herein, thus showcasing NBC advancement. The experimental solving of another problem called as the Satisfiability problem, has also been presented here. The results emphasize the ability of NBC to solve multiple NP-complete problems by developing new algorithms.

However, we also identify limitations, particularly increased error rates caused by cytoskeletal filaments taking incorrect turns at junctions. Increase in problem size is directly proportional to the complexity of the maze network leading to additional opportunities to take wrong turns. Higher error rates of cytoskeletal filaments hinder scalability for larger problems. This thesis also presents a strategy to overcome the above problem by optimizing pass junctions, considering factors such as width and turn angles. These optimized junctions facilitate high performance resolution of even large-scale problems. Additionally, the thesis introduces the concept of 3D junctions, represented by tunnels and bridges, which can eliminate turns and generation of errors.

Further, I will outline several other essential technical prerequisites essential for the continued scaling up of NBC such as (i) cheap and mass production of nanodevices; (ii) self-multiplication of agents; and (iii) continuous supply of agents to the nanodevices. These requirements are not addressed within the scope of this thesis.

List of Papers

Paper I

Salhotra, A.; Zhu, J.; **Surendiran, P**.; Meinecke, C. R.; Lyttleton, R.; Ušaj, M.; Lindberg, F. W.; Norrby, M.; Linke, H.; Månsson, A. **Prolonged Function and Optimization of Actomyosin Motility for Upscaled Network-Based Biocomputation.** New J. Phys. 2021, 23 (8), 085005. https://doi.org/10.1088/1367-2630/ac1809.

I designed and performed the device fabrication and surface modification, and performed the motility assay experiments jointly with J. Zhu and A. Salhotra and performed the analysis of these devices. I contributed to the writing and editing of the paper.

Paper II

Surendiran, P.; Meinecke, C. R.; Salhotra, A.; Heldt, G.; Zhu, J.; Månsson, A.; Diez, S.; Reuter, D.; Kugler, H.; Linke, H.; Korten, T. **Solving Exact Cover Instances with Molecular-Motor-Powered Network-Based Biocomputation.** ACS Nanosci. Au 2022, 2 (5), 396–403. https://doi.org/10.1021/acsnanoscienceau.2c00013.

I designed the actin-myosin experiments together with the co-authors. I fabricated and surface-functionalized the samples. I performed the motility assay experiments and imaging together with A. Salhotra. I performed the analysis of the actin-myosin data. Statistical analysis was performed by T. Korten. I wrote sections describing actin-myosin experiments.

Paper III

Zhu, J.; Salhotra, A.; Meinecke, C. R.; **Surendiran, P**.; Lyttleton, R.; Reuter, D.; Kugler, H.; Diez, S.; Månsson, A.; Linke, H.; Korten, T. **Solving the 3-Satisfiability Problem Using Network-Based Biocomputation**. Adv. Intell. Syst. 2022, 4 (12), 2200202. https://doi.org/10.1002/aisy.202200202.

I contributed to the fabrication and surface functionalization of the devices. I performed motility assay experiments and imaging together with A. Salhotra. I contributed to the editing of the paper. Network algorithm development and statistical analysis were performed by J. Zhu and T. Korten.

Paper IV

Surendiran, P.; Ušaj, M.; Korten, T.; Månsson, A.; Linke, H. Error-rate reduction in network-based biocomputation

Manuscript

I co-designed the project with the co-authors and conducted all the experiments and simulations using code developed by T. Korten and A.Månsson. I performed the device fabrication and surface functionalization. I contributed to motility assay experiments and imaging together with M. Ušaj. I carried out the data analysis. I wrote the paper with input from the co-authors.

Paper V

Reuther, C.; Steenhusen, S.; Meinecke, C. R.; **Surendiran, P**.; Salhotra, A.; Lindberg, F. W.; Månsson, A.; Linke, H.; Diez, S. **Molecular Motor-Driven Filament Transport across Three-Dimensional, Polymeric Micro-Junctions**. New J. Phys. 2021, 23 (12), 125002. https://doi.org/10.1088/1367-2630/ac39b4.

I adapted the device design for the study of the actin-myosin system. I performed the surface functionalization of the devices fabricated by S. Steenhusen and analysis of the results. I performed the motility assay experiments and imaging together with A. Salhotra. I contributed to the editing of the paper.

Related publications outside the scope of the thesis

Paper VI

Unksov, I. N.; Korosec, C. S.; **Surendiran, P**.; Verardo, D.; Lyttleton, R.; Forde, N. R.; Linke, H. **Through the Eyes of Creators: Observing Artificial Molecular Motors.** ACS Nanosci. Au 2022, 2 (3), 140–159. https://doi.org/10.1021/acsnanoscienceau.1c00041.

Paper VII

Korosec, S.; Unksov, I.N.; **Surendiran, P**.; Lyttleton, R.; Curmi, P.M.G.; Angstmann, C.N.; Eichhorn, R.; Linke, H.; Forde, N.R. **The Lawnmower: An Autonomous, Protein-Based Artificial Molecular Motor.**

Preprint: https://arxiv.org/ftp/arxiv/papers/2109/2109.10293.pdf

Under revision in Nature Communications

Paper VIII

Salhotra, A.; Rahman, M. A.; Ruijgrok, P. V.; Meinecke, C. R.; Ušaj, M.; Zemsky, S.; Lindberg, F. W.; **Surendiran, P**.; Lyttleton, R. W.; Linke, H.; Korten, T.; Bryant, Z.; Månsson, A. **Exploitation of Engineered Light-Switchable Myosin XI for Nanotechnological Applications**. ACS Nano 2023. https://doi.org/10.1021/acsnano.3c05137.

Abbreviations

ADP	Adenosine diphosphate
ALD	Atomic layer deposition
ATP	Adenosine triphosphate
DNA	Deoxyribonucleic acid
F-actin	Filamentous actin
G-actin	Globular actin
HMM	Heavy meromyosin
EBL	Electron beam lithography
ExCov	Exact Cover problem
IVMA	*In-vitro* motility assay
P	Polynomial
NBC	Network-based biocomputation
NP	Non-deterministic polynomial time
PA	Plasma ashed
SAT	Satisfiability problem
SEM	Scanning electron microscopy
SSP	Subset sum problem
TMCS	Trimethylchlorosilane

Acknowledgments

Embarking on a journey that spanned continents, driven by a dream that was once distant, I have come to realize that transforming that dream into reality is a collective endeavour. I am deeply grateful to all the remarkable individuals who accompanied me on this journey.

Foremost, I extend my heartfelt gratitude to my supervisor, Heiner Linke, for entrusting me with this exceptional opportunity. Your unwavering support, guidance, and invaluable insights have been the cornerstone of my doctoral journey. Your leadership acumen and adeptness in managing diverse challenges have been a true inspiration. The constructive feedback you provided has been instrumental in my professional growth, and for this, I am profoundly thankful.

To my co-supervisor, Alf Månsson, I extend my thanks for being a steadfast pillar of support. Your expertise and timely solutions to every encountered obstacle have been invaluable. Your kindness and approachability have made our collaboration a truly enriching experience.

The EU project Bio4Comp has been a privilege to be a part of, introducing me to a team of exceptional professionals. Special thanks go to Till Korten, whose extensive expertise within the project has been a guiding light. To Christoph Meinecke, Cordula Reuther, Sönke Steenhusen, and the other members of Bio4Comp, it has been a pleasure working alongside you, and I extend my gratitude for your unwavering support. In the laboratories of Kalmar, my colleagues and friends have been indispensable. Marko and Aseem, your dedication to research and ability to find solutions during challenging times have been truly inspiring. This work would not have been the same without you.

Jingyuan Zhu, your role as a colleague, friend, and mentor has been invaluable. I am grateful for the insightful discussions, collaborative experiments, and help that shaped this journey. I would like to thank Vanya and Therese, who have been with me throughout this Ph.D. journey, for their unwavering professional and personal support. Ruby, Julia, Patrik, Mariia and Michael, your positivity, engaging discussions, and readiness to assist have been uplifting. It has been a pleasure getting to know you. I extend my thanks to the group's former and newest members: Roman, Frida.L, Damiano, Zeus, Nils, and Mikkel. To Esra, Elham, Enrico, Frida, Jason, Christelle, Jonas, and all the former members of the biogroup, I am grateful for the stimulating conversations and shared positivity.

The technical and administrative help I received on a daily basis was pivotal. It is impossible to enumerate all those who played a part, but I am deeply grateful for their unwavering support. I would like to thank my office mates Max, Martin, and Chun Lin, with whom I had conversations that have constantly kept the work environment pleasant. To all my wonderful colleagues at the division: Alexander,

Alexandra, Alfons, Anastasiia, Anders G, Anders K, Andreas, Anette, Anna-Karin, Antti, Asmita, Bengt, Carina, Dan, Dmitry, Gerda, Hossein, Håkan, Kristi, Luke, Maria, Marica, Marie, Mirja, Sebastian, Thanos, Therese S, Yue, and the list goes on, thank you for all the conversations filled with fun and support.

During my time in Sweden, I have met some incredible people whose friendships have made my past five years truly memorable. Loki and Aaron, thank you for always being there for me through the good and bad times. The memories we've created together are countless and cannot be fully articulated in just a few sentences, and I look forward to making many more unforgettable memories. Uthira, Jenny, and Reshma, I have thoroughly enjoyed spending time with you all. Our moments together have been filled with laughter and joy, and Uthira, I am especially grateful for all the support, especially during my past two years in Lund. To Yamini chechi, Heera, and Carina chechi, you have all been like sisters to me. Your kindness and companionship have made my time in Sweden incredibly comfortable and enjoyable.

A special thanks to my family. I want to thank Poornima chechi and my mother-in-law, Jayashri. You embraced me and listened to all my problems with open minds, always offering your support with warmth. Veliamma, thank you for always being a part of my life. To my little sister, Arunima, thank you for always saying the things I needed to hear and comforting me. Not all heroes wear capes, and that's my mother, Bhuvaneswari, and father, Surendiran. This note of thanks cannot encompass the depth of gratitude I feel for everything you have given me. Thank you for your sacrifices to shape me into who I am today. Lastly, to my beloved husband, Puneet, you have been my solid support on this journey. Without you, I wouldn't have come this far. Thank you for patiently listening, inspiring, and for loving me as you do.

1. Introduction

Semiconductor technology, guided by the International Technology Roadmap for Semiconductors (ITRS)[2] and described by Moore's law[3], has resulted in the development of remarkably reliable and high-speed electronic processors. Nevertheless, the continuous progress faces challenges due to the increasingly excessive power consumption linked to escalating heat dissipation[4]. The potential to decrease energy dissipation, such as through further miniaturization of electronic components, faces constraints imposed by physical size limitations[5] and the complexities associated with heat management. Due to these constraints, electronic computers that operate serially have limitations in solving combinatorial mathematical problems, specifically nondeterministic polynomial-time complete (NP-complete) problems. These problems are a class of computational problems for which no known efficient algorithm is available[6]. These problems are relevant in real-world applications such as data clustering[7], and protein design[8].

Problems categorized as tractable can be solved using computer algorithms operating within polynomial time. For a problem of size n, the time or steps required to obtain a solution follow a polynomial function with n. Conversely, NP-complete problems are considered intractable as they demand resources characterized by exponential functions of the problem size n. Algorithms that operate within polynomial time are viewed as efficient. In contrast, those in exponential time are considered inefficient due to their significantly exponential growth in execution times and energy consumption as the problem size increases[9,10]. Consequently, there is a need for efficient parallel computing approaches where multiple processors work simultaneously and independently. This has an energetic advantage for large-scale problems dissipating less energy and less time consumption compared to serial computing[4]. As a result, researchers have been exploring alternative parallel computing methods, including DNA computation[11–13] and quantum computation[14–16]. However, each of these approaches faces unique challenges that currently restrict their practical implementation.

In recent years, a third parallel computation approach known as network-based computation (NBC) has been developed. In NBC, the problem instance was encoded into a two-dimensional network, where cytoskeletal filaments propelled by molecular motors traversed a series of junction crossings and ultimately collected at exits representing the solutions of the problem. The fundamental components and overview of a typical NBC device are illustrated in Figure 1.1. The key sections of

the device include (i) an inlet serving as the source of motile agents required for computation, (ii) a 2D network encoded with the mathematical problem, leading to exits that correspond to potential solutions for the given instance of problem, (iii) junctions serving as regulatory geometries designed to control the movement of cytoskeletal filaments within the network, ensuring directed and controlled traversal, and (iv) readout regions where the cytoskeletal filaments reaching different exits are detected and counted to determine the solutions.

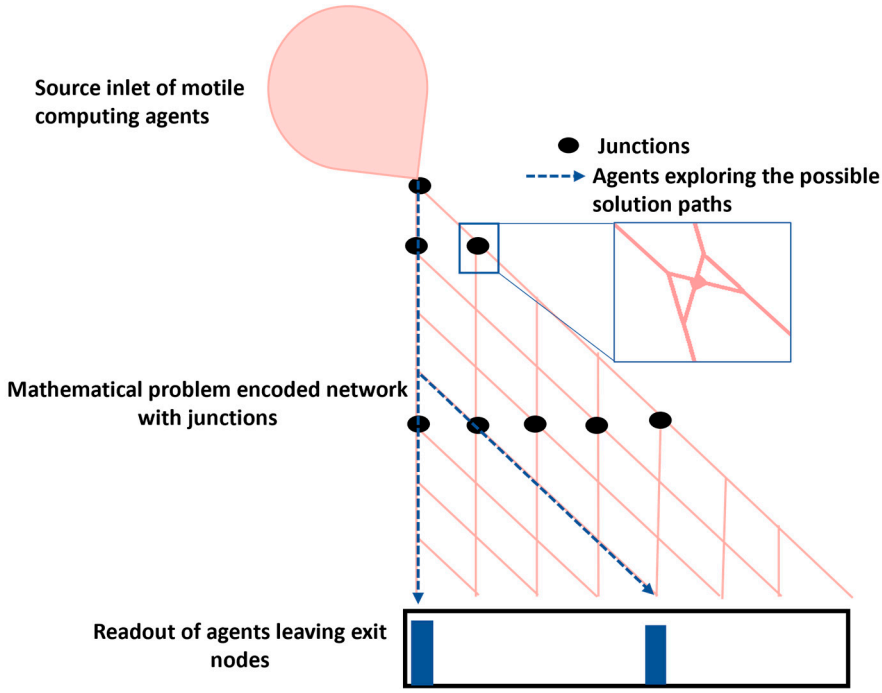

Figure 1.1: Schematic of a generic NBC device. The motile agents enter the directed network from a large inlet which is the source of agents. They enter a problem-encoded network where their movement is regulated by geometries called junctions. They finally leave the network through the exit which corresponds to the solutions and the filaments exiting are detected to analyze the solution of the problem. Each possible path through the network corresponds to one solution of the solution space. [Source: schematic figure drawn based on the SSP network[17]]

Molecular motors, a class of proteins found in biological systems, harness the chemical energy of ATP to perform various functions[18–20]. Notable examples of molecular motors include the kinesin family[18,21] and myosin family[18,22], which convert the chemical energy stored in ATP molecules into mechanical motion. These molecular motors play vital roles in cellular functions, such as muscle contraction, cellular and intracellular transport[18,19,23]. A detailed description of the actin-myosin II system used in the thesis will be further discussed in Chapter 2.

Within NBC, molecular motors operate logically at much lower clock frequencies (only a few Hz) compared to electronic processors (GHz), which means that they can operate with less energy per computation. By using a high degree of parallelism, they can thus solve, in principle, the same problem at the same time in an energy-efficient manner. In a proof-of-concept experiment, NBC was used to solve a small instance of the NP-complete subset sum problem (SSP) using molecular systems such as actin-myosin and microtubule-kinesin[17]. The high energy efficiency and parallel operation of molecular motors in NBC were shown to result in several orders of magnitude lower energy consumption per operation when compared to electronic computers[17].

The nanodevices used in NBC are fabricated by a combination of two steps, as depicted in Figure 1.2: (i) physical patterning of the structures using electron beam lithography (ii) chemical modification of the devices using oxygen plasma treatment and surface functionalization (e.g., silanization) for selective attachment of molecular motors.

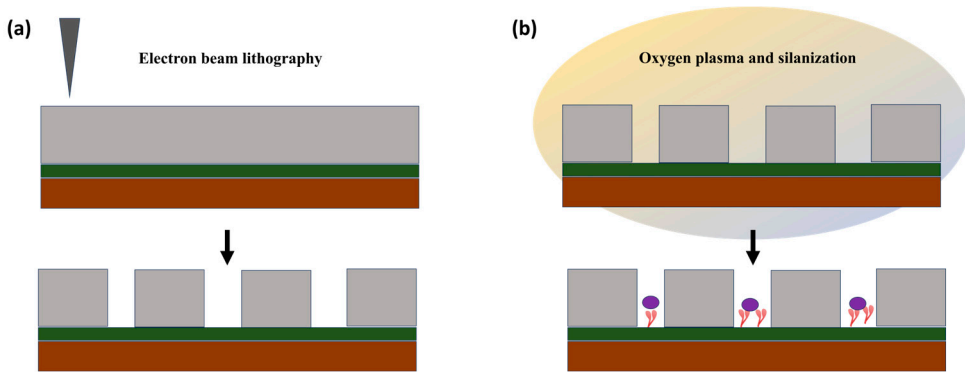

Figure 1.2: Schematic illustration of (a) Electron-beam lithography used for fabricating the structures (b) Surface functionalization of the devices for proper attachemnt of molecular motors (in orange) enabling selective motility of the computational agents (i.e. actin filaments or microtubuli, represented as purple circles).

Various pre-requisites[24,25] addressed in this thesis for scaling-up NBC as a competitive technology are given below:

- Development of stable operation and standardization of nanodevices using fabrication and surface functionalization.
- Solving multiple combinatorial problems using newly developed algorithms.
- Addressing the major limitation of error rates in junctions.

The thesis focusses on addressing these requirements. The optimization and troubleshooting of the parameters used in the fabrication and surface functionalization of NBC devices are described (Paper I). Factors affecting actin-myosin longevity in the fabrication of NBC devices are evaluated for stable operation. As a result, the actin-myosin function in these devices increased from <20 min to >60 min.

Utilizing the optimized process parameters obtained from Paper I, solutions are put forward for two other NP-complete problems, Exact Cover and Satisfiability. These solutions were achieved by using new algorithms developed by collaborators. The experimental solving of different instances of these problems are described in Paper II and III. Furthermore, the studies emphasize the significance of developing new algorithms as a key advancement in solving multiple combinatorial problems using NBC.

At traffic-regulating junctions, the agents are expected to move in a straight direction as its initial path, without deviating. If an agent deviates from the prescribed direction, it will ultimately arrive at an incorrect solution exit, leading to an inaccurate count at that exit which is considered an error. The junction geometry parameters were systematically modified to explore different designs aimed at reducing error rates. Experimental investigations carried out, resulted in an optimized junction geometry with an error rate less than 1% compared to the state of the art error rate of 2-4%[1,17] (Paper IV). This would enable the scaling up of network sizes from tens to hundreds of pass junctions[24]. By incorporating a molecular motor layer in the simulation model of filaments within a channel, the fit between experimental and simulated results improved.

Complete error mitigation requires creation of three-dimensional junctions in the shape of tunnels and bridges. As an initial demonstration, attempts have been made using two-photon polymerization to explore such an approach (Paper V). The early findings indicate the feasibility of developing photo-polymerizable inorganic-organic hybrid polymer (ORMOCER®) based 3D junctions for the actin-myosin system. To summarise, the advancements introduced in this thesis mark a progression towards optimized and scaled-up biocomputing networks designed to tackle more combinatorial problems through parallel processing, thus ensuring enhanced energy efficiency. Nonetheless, numerous pre-requisites remain to be met to realize the future scalability of NBC devices for competitive problem-solving in comparison to electronic computers. Some of the future milestones to be addressed include:

a) Electron beam lithography is a time-consuming and expensive method to fabricate devices. To tackle this issue in the future, other cost, and time-efficient lithography techniques like Nanoimprint lithography (NIL) may be employed to fabricate multiple identical devices at the same time.

b) As the size of the mathematical problem increases, the number of agents needed to solve it also grows exponentially. This challenge could be overcome through the self-multiplication of filaments, achieved by splitting the filaments and then adding monomers for subsequent growth.

c) Currently, readout of the devices is executed using imaging of fluorescently labelled filaments. This will ultimately become limited by the field of view as the devices scale-up. A probable detection method would be a real-time direct readout of the filaments via electrical detection employing nanoscale field-effect transistors.

d) Continuous supply of agents and energy in the form of ATP is an important requirement to achieve prolonged operation of the NBC devices. This can be achieved by embedding the NBC chips in microfluidic devices where the chips can be fed using reservoirs and channels.

The remaining thesis is structured as follows:

Chapter 2 pertains to the nature of combinatorial problems and the necessity of parallel computation to solve them. It also explains NBC's functioning and its application in solving Subset sum problem.

Chapter 3 focuses on the design and development of NBC devices, including a detailed description of the electron beam lithography technique employed for nanodevice fabrication and the optimization of process parameters. It also elucidates the surface functionalization technique used for selective motility of filaments in nanochannels. Further, optimization of parameters to ensure desired biocompatibility between devices and molecular motors are also elaborated.

Chapter 4 illustrates the experimental demonstration of solving the Exact Cover problem and Satisfiability, two other combinatorial problems. It presents the scalability achieved and observations derived from solving these problems using NBC.

Chapter 5 addresses the vital challenge of error mitigation in NBC scaling-up. It discusses two distinct approaches employed to overcome this challenge namely 2D junction geometry optimization and 3D junction development.

Chapter 6 presents the significant conclusions drawn from the thesis research and offers an outlook on potential future developments in the field of NBC.

2. Solving combinatorial problems

In this chapter, we introduce combinatorial problems and their significance. We present three examples: Subset sum, Exact Cover, and Satisfiability. We also briefly cover alternate parallel computing techniques like DNA computation and quantum computation. We introduce 'Network-based biocomputation' which uses molecular motors.

2.1 NP-complete problems

To understand NP-complete problems, the concepts in relation to them are discussed here:

Decision problems: A 'problem' is a general question with a set of unspecified parameters that requires an answer. An 'instance' of a problem occurs when specific values are assigned to these parameters. Decision problems are a class of mathematical problems that have two possible solutions of 'yes' and 'no' for an instance of the problem under certain rules[6]. As the problem size and number of variable inputs increase, the solution space increases exponentially. The algorithms used to solve these problems could be either polynomial time algorithm or exponential time algorithm[6].

Time complexity: Time complexity measures the amount of computational time an algorithm takes to run, as a function of the size of the input to the algorithm[6]. When the problems are solved in polynomial time functions such as $f(n)= n^x$ where n is the number of inputs and x is a positive integer, they are called P problems. For example, finding the determinant of a matrix can be done in polynomial time function, n^3. This means that a polynomial time algorithm exists for a given problem instance. On the other hand, some problems usually need an exponential time-costing algorithm which takes an exponential function, say 2^n or 3^n time to solve them where n is as before the number of inputs[2]

NP problems: Non-deterministic polynomial time (NP) problems are a class of decision problems where when a potential solution is determined, it can be verified to be correct in polynomial time. In mathematics, the question of whether there exists a polynomial time algorithm to solve this problem is of great interest. Some of the particularly hard NP class problems can be classified as NP-complete

problems. These problems possess multiple solutions that cannot be solved in polynomial time, but they can be verified within polynomial time. Finding solutions for NP-complete problems requires exponential time and energy resources.

Reduction: The theory of 'polynomial time reducibility' validates that, if a polynomial time algorithm is developed for one NP-complete problem, any other NP-complete problem can be converted and solved using a corresponding polynomial time algorithm[26]. If an optimized algorithm is developed for one problem, then that can be converted to solve other NP problems[26,27].

Real-world significance: Many of the NP-complete problems of interest to solve real-world problems such as airplane fleeting[28], resource allocation[29] and cryptography[30] are combinatorial in nature which means the solution of these problems is found from a finite set of objects by satisfying the given conditions.

Classical computers employ sequential algorithms that require exponential time and energy to solve NP-complete problems. Thus, there arises a necessity for parallel computation techniques, wherein multiple tasks are executed simultaneously to reduce the energy cost per operation. This is supported by studies indicating that the time and energy cost per operation in parallel computing remains independent of the problem size[4]. Some examples of combinatorial problems of interest covered in this thesis and describe below include Subset sum problem (SSP), Exact Cover (ExCov), and Satisfiability (SAT).

2.1.1 Subset Sum Problem

The first proof of concept problem solved by the method of NBC was an instance of SSP[17] which will be described in this Chapter. SSP asks to find all possible sums when a set of integers is given[6,31]. The time complexity of these problems vary based on the instances of the problems and the existence of efficient algorithms for solving these problems[32,33].

SSP is mathematically defined as:

Given a set of positive integers $S=\{a_1,a_2,\ldots, a_N\}$ of N integers, the goal is to determine if there exists a subset of S such that the sum of its elements equals to target sum, T. The question is whether there is a solution $\sum_{i=1}^{N} yisi$ where yi ∈ {0, 1}, for any given T from 0 to $\sum_{i=1}^{N} si$

This problem will be classified as NP-complete if there exists no efficient algorithm because, the time to find all combinations of integers scales exponentially with a time function of 2^n. One of the main applications of SSPs is in the field of cryptography[30].

2.1.2 Exact Cover

The Exact Cover (ExCov) problem determines a subset of elements from a given collection such that each element is selected only once and specific conditions are met. This problem aims to find out if an exact cover exists for a collection S of subsets for a given set X. The exact cover is a subcollection of subsets S' which contains each element of X only once.

For example, X= {1, 2, 3, 4} and the collection of subsets S= {(3,4),(2,4),(2,3)(1,3)}, then the exact cover of this problem is S'={(1,3),(2,4)}.

There are many algorithms developed to solve these problems, of which an algorithm called DLX using specific data structures (Dancing links)[34] is widely used for solving ExCov in real-world applications such as air fleet planning[28]. However, the computational time and cost of these algorithms are exponential. There have been efforts to solve them using other parallel computing techniques like quantum computing but they are also limited by error and scalability issues[16]. In this thesis, we will be focusing on solving instances of ExCov using the NBC approach.

2.1.3 Satisfiability problem

Boolean satisfiability is a decision problem that is very significant in the theory of NP-completeness for transformations of the algorithm to other basic NP-complete problems. The main goal is to find an assignment of variables to TRUE or FALSE so that the given Boolean formula is satisfiable. Here are some key elements and symbols commonly associated to understand the Boolean Satisfiability Problem:

Boolean Variables (x, y, z, etc.): These are variables that can take on one of two logical values: true (T) or false (F). In formal notation, these are often represented as $x1$, $x2$, $x3$...

Logical Operators: (i) AND **(∧):** Represents logical conjunction. $x \wedge y$ is true only when both x and y are true. (ii) OR **(∨):** Represents logical disjunction. $x \vee y$ is true when at least one of x or y is true. (iii) NOT **(¬):** Represents logical negation. $\neg x$ is true when x is false.

Boolean Expressions: These are combinations of Boolean variables and logical operators. For example, $x \vee (y \wedge \neg z)$ is a Boolean expression.

Clauses: A clause is a disjunction (OR) of literals. For example, $x \vee \neg y \vee z$ is a clause.

Conjunctive Normal Form (CNF): A Boolean formula is said to be in CNF if it is a conjunction (AND) of one or more clauses. For example, $(x \vee y) \wedge (\neg x \vee z)$ is in CNF.

Satisfiability (SAT): Given a Boolean formula in CNF, the SAT problem is to determine if there exists an assignment of true values to the variables that makes the formula true.

Satisfying Assignment: If there exists an assignment of truth values to the variables that makes the formula true, this assignment is called a satisfying assignment.

Unsatisfiable: If no such assignment exists, the formula is said to be unsatisfiable.

For example, there are two clauses with 3 variables as given below.

$$(x_1 \vee x_2 \vee x_3) \wedge (x_4 \vee x_5 \vee x_6)$$

This Boolean expression in 3-SAT form has 2 clauses with each clause containing 3 variables. The question is the same, are there such values of $x_1 ... x_6$ such that the given Boolean expression is TRUE?

They play a prominent role in technologies such as planning in network routing[35]. This is one of the widely explored problems as it was the first problem to be proven as NP-complete[6,27]. The reducibility of NP-complete problems shown by the Karp's theorem starts with 3-SAT problems which are then reduced to other problems[26]. Currently, there is no polynomial-time algorithm that can efficiently solve this problem. The parallel computing method of DNA computing has been used to solve this problem but is limited by several factors such as errors caused by false positives and the need for a high amount of DNA[13].

2.2 Alternate parallel computation techniques

2.2.1 DNA computation

DNA computing solves mathematical problems by using single strands of DNA made of unique oligonucleotide sequences as computing agents which results in the desired solution when combined with complementary strands[11,12]. The remaining excess single-stranded DNA is removed from the solution and further, the solution strands are extracted, and amplified to determine the answer to the problem. There are several DNA algorithms to solve different NP-complete problems which have shown the potential for data storage capability and energy efficiency[13,36,37]. In recent studies, DNA computing has been used to solve practical optimization problems such as traveling plans for several families to multiple cities with minimum cost[38] and in graph theory[39]. However, the algorithm implementation is limited by the coding ability and computational simulation to verify the algorithms developed[40]. Furthermore, the scalability of this approach is limited by the need for a high amount of DNA quantities that increase dramatically[41] with more complex problems and

increased error rates caused by breakage of strands and false positives in computation[42,43].

2.2.2 Quantum computation

Quantum computing uses the quantum mechanical superposition of dual states of quantum bits or “qubits” as computing agents. The innate properties of entanglement and superposition of qubits allow for large parallelism in computation[14,44,45]. Algorithms developed for implementing quantum computing include Shor’s algorithm[46,47], quantum annealing[14,45,48], and adiabatic quantum computation[45,48]. The two main obstacles in quantum computing are 'decoherence' and the optimization of computational architecture needed to control the qubits[15,46,47,49]. Therefore, only solving small instances of problems by quantum computation has been demonstrated so far[7,15,45]. IBM Osprey, a 433-qubit quantum processor is currently the world largest processor. IBM has released a roadmap where they aim to build 1 million qubit quantum system in the coming years with better infrastructure for error correction[50].

2.3 NBC using molecular motors

The working and different components of NBC is explained in this section.

2.3.1 Computing agents

2.3.1.1 Actin-myosin system

The actin-myosin molecular system used for NBC in this thesis is isolated from rabbit skeletal muscle. Skeletal muscle is comprised of myofibrils, which are built of repeating sarcomere units containing myosin, actin, and other proteins[51,52]. The arrangement of actin filaments around the myosin filament with protruding myosin motor heads enables the cross-bridge cycle, which is integral to muscle contraction[51,53,54]. This mechanism is responsible for the actin filaments sliding over the myosin heads in the muscle during contraction. Actin filaments (F-actin) are a product of the polymerization of globular monomers (G-actin) helically arranged such that the filaments have polar charges. The length of the filaments is typically several micrometres (μm) and the diameter is around 10 nanometers (nm)[51,55]. The main features of the actin-myosin system include the actin filaments propelled at high velocities of 10 μm/s[56,57] and that the actin filaments are flexible with a persistence length of 10-20 μm[56,58]. This persistence length is a key factor that determines the filament's flexural rigidity.

The regulation of muscle contraction is via calcium binding to troponin, which effectively changes the tropomyosin conformation on the actin filaments and exposes the myosin binding sites. Then the myosin heads undergo a conformational change which is responsible for pulling the actin filaments forward. ATP hydrolysis is a process where the ATP molecule is converted to ADP and an inorganic phosphate ion. The energy released is responsible for the conformational changes in the myosin heads in the cross-bridge cycle[55,59,60]. For every ATP molecule, the cycle is repeated, and a force is created which acts on the actin filament that makes a step forward over a distance of 10-28 nm[22,59]. Each step consumes one ATP molecule and uses energy of around $20kT$[56,61] with a thermodynamic efficiency of around 50%. Moreover, myosin II enables the propulsion of actin filaments at high speeds, reaching approximately 10 μm/s[56]. In this thesis work, we used a class of myosin called myosin II[62]. Particularly, we have used only a portion of myosin II, namely heavy meromyosin (HMM) which provides the functionality of actin sliding.

2.3.1.2 Microtubule- kinesin system

Another important molecular motor system used for NBC is the microtubule-kinesin system. They are also widely used for similar applications as the actin-myosin system. Microtubules are hollow tube helical structures made of tubulin protofilaments arranged to form stiff filaments[63,64]. They have a diameter of around 25 nm with lengths as long as 60 μm[58] and a persistence length of several millimeters[58,65] making it much bigger and firmer in comparison to the actin-myosin system. Their persistence length could be reduced to μm when transported using kinesin motor proteins. Inside the cells, kinesin-I motor is used for cargo transportation along the microtubules. They are adapted for microtubule movement by utilizing ATP hydrolysis and cyclic interactions with the microtubule similar to the actin-myosin system[21]. Kinesin-I mediated microtubule movement is slower than actin-myosin with a velocity of 1 μm/s[17].

2.3.2 Solving SSP using NBC

The first biocomputation device was fabricated to solve an instance of NP-complete problem, subset sum problem (SSP) with eight possible solutions using molecular motors where the mathematical problem was encoded into a physical network with junctions and channels[17]. In general, the problem layout varies depending on the specific inputs for a given problem instance.

As an example, in Figure 2.1, given is the SSP instance of (2, 3, 7). The possible sums and correct solutions are then corresponding to (0), 2, 3, 5,7, 9, 10, 12. This problem is encoded into a physical network in which the directional motion of filaments represents addition. The filaments enter from one corner of the network and move through the network passing through network junctions called ‘pass’ and

'split' junctions as shown in Figure 2.1. The pass junctions allow the filaments to only move with a directed onward motion to the next junction retaining the initial direction whereas, the split junctions allow the filaments to take turns which defines their future path.

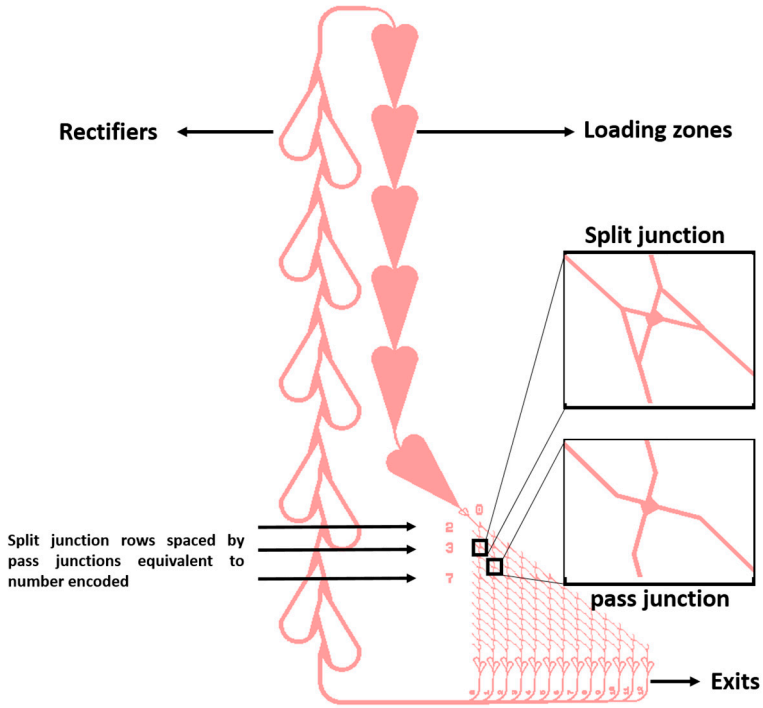

Figure 2.1: Schematic layout of an NBC network of an instance of the subset sum problem encoding the numbers (2, 3, 7). The filaments enter the network with pass and split junctions from large areas of inlets called loading zones that act as storage for the filaments. Split junctions are placed with spacing equivalent to the number of pass junctions which depends on the number encoded. Rectifiers allow the filaments to return to the network. The possible solutions are determined by the paths taken by the filaments in the network and the filaments are collected at the exit row.

The position of the split junctions is significant as this defines the numbers encoded into the network while also determining how far the filaments move in the network and when they are supposed to take turns. The spacing between the split junction rows is determined by the number that needs to be encoded which is unique for a given instance of the problem. When the agents move downward from a split junction without crossing it diagonally, there is no summation whereas the diagonal movement is equivalent to summation as shown in Figure 2.2. The more diagonal

turns the filaments take, the higher the sum it exits at. The number of pass junctions between the rows of split junctions is equivalent to the number encoded as depicted in Figure 2.2. The solution exits represent the target sums which get higher as it is laid further to the right.

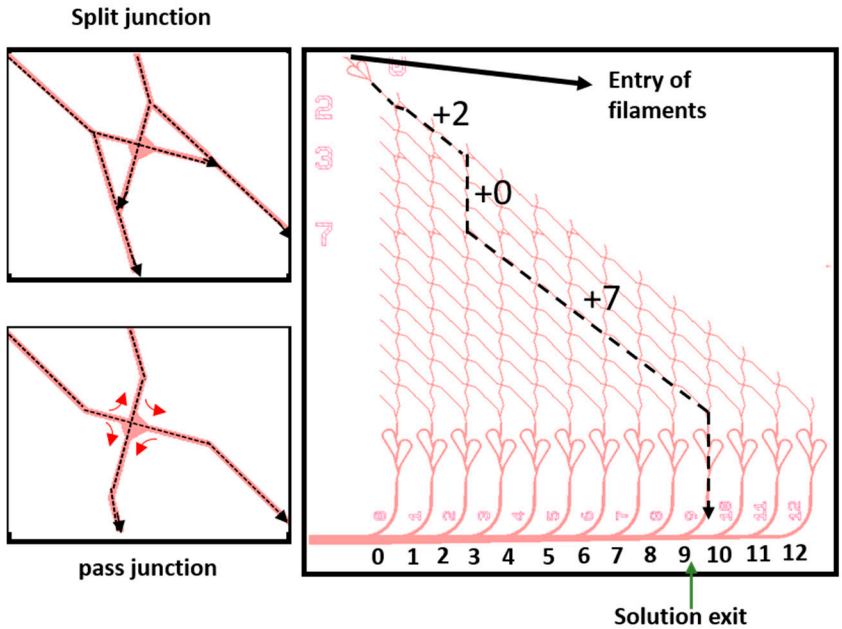

Figure 2.2: Path of filaments in the pass and split junctions. The dotted lines show the allowed movement of filaments in these junctions and the red arrows indicate the paths they are not allowed to move and can contribute to the error of the system if they take these paths. On the right, filaments are shown to reach the solution exit by biocomputation. Diagonal paths represent summation, and no number is added when the filaments move straight downward. Here, the solution exit 9 is reached by summation of 2 and 7 as the filaments take a diagonal path at the split junctions corresponding to it.

The mechanical self-propelled movement of the filaments, powered by energy released upon ATP hydrolysis, demonstrates remarkable energy efficiency. The Landauer limit represents the fundamental limit of energy consumption and heat generation for computation which is given as kTln 2 per binary operation, where k is the Boltzmann constant and T the temperature[4,66]. At room temperature, the Landauer limit is calculated to be 2.9×10^{-21} J. This can be used as a benchmark to evaluate the energetic advantage of NBC. A single operation in NBC can be considered as the movement of filament between two subsequent split junctions[17]. The energy cost for this operation for NBC is calculated to be ~10^{-14} J[17] which is hundreds of magnitude lower than the advanced electronic computers[67].

3. Nanodevice development

This chapter focuses on developing nanodevices for NBC, explaining their fabrication using electron beam lithography and surface functionalization for selective guidance of computing agents. It also addresses challenges in operating the devices for extended periods and optimizing important parameters for improved performance and run-time.

3.1 Fabrication

3.1.1 Layout design

The NBC devices are designed and processed to get a controlled and guided motion of the filaments along the problem-encoded channels. Their movement is restricted by forming channels with walls. The channels are designed based on the persistence length and size of the cytoskeletal filaments as they determine the dimensions of the networks. As discussed above in section 2.3.1, actin filaments have a lower persistence length which makes them more flexible compared to microtubules. Thus the actin filaments need a smaller channel size of less than 300 nm for guided motion, whereas the microtubules are better guided in wider channels of approximately 1μm. The height of the channel walls for the actin-myosin devices is around 200 - 300 nm. The overall layout of the NBC device depends on the graphical network specific to the problem and includes all the essential components as described in section 2.3.2. NBC devices should be fabricated using high-precision lithography techniques such as electron beam lithography (EBL)[68,69] and nanoimprint lithography[70] to construct sharp features of nanometer size. In our work, EBL was used for fabricating all the devices.

3.1.2 Electron-beam lithography

The process of EBL involves the use of high-energy electrons to modify the solubility of electron-beam-sensitive film coated on a surface. Upon exposure to the electron beam, the solubility of the film is altered, allowing for etching away the exposed regions using a chemical solvent known as developer. EBL is a maskless

lithography technique that enables patterning with high resolution, achieving sub-10 nm resolution[69]. The high resolution and precision achieved through EBL is crucial for the fabrication of structures with very small features and has a significant impact on device performance. However, scanning of the pattern to the substrates during EBL leads to longer exposure times and low throughput. This is due to the creation of patterns through the alignment and stitching of different scan areas to produce a single pattern. Any imprecision in the deflection of the electron beam during this process can cause broken structures and proximity effects, which are dependent on the exposure parameters[68,69].

3.1.3 Fabrication of NBC devices

For fabricating our NBC devices, 10 × 8 mm^2 Si(100) chips were used as device substrates. A 75 nm thick silicon dioxide (SiO_2) on the silicon (Si)-substrate was prepared by thermal oxidation shown in Figure 3.1 A. The SiO_2 substrates were cleaned in acetone and isopropanol for 3 min each in an ultrasonic bath at room temperature followed by drying under nitrogen flow and plasma cleaning to remove all organic and inorganic debris. Here, CSAR62, a high-resolution EBL resist was spin-coated to a thickness of around 200-300 nm on the cleaned substrate and baked on a hotplate at 180 °C for 120 s was used (Figure 3.1 B). The network was patterned by EBL as depicted in Figure 3.1 C. The chips were then developed using the developer amyl acetate for 90 s and rinsed in IPA for 30 s. Thus, the formed network channels as shown in Figure 3.1 D provide physical guidance to the filaments.

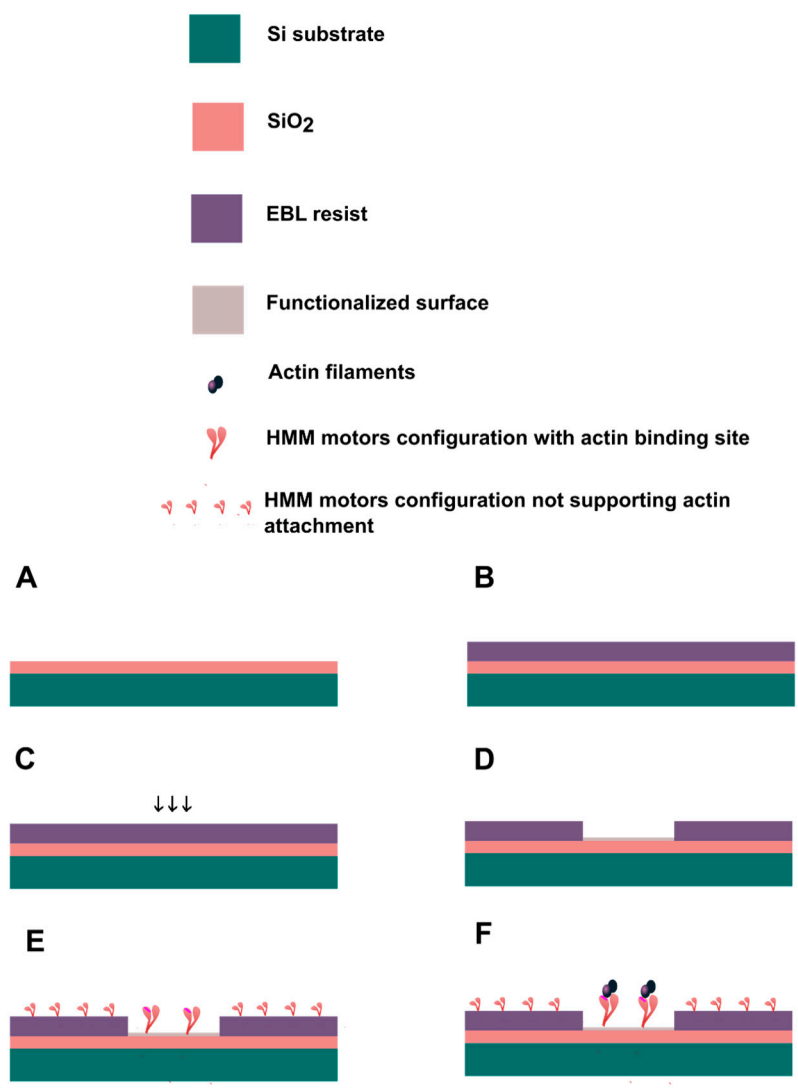

Figure 3.1: Schematic of the fabrication and surface functionalization process (A) SiO_2 layer formed on the Si-substrate is cleaned and baked for further processing. (B) Spin coating of EBL resist onto the prepared surface is performed followed by baking on hotplate to dry the resist before processing. (C) EBL patterning changes the solubility of the resist corresponding to the network pattern. (D) The exposed regions are developed and activation of the exposed SiO_2 surface is done by plasma ashing and TMCS silanization. (E) Hydrophilic regions of the resist make the HMM motors in a configuration not supporting actin attachment and hydrophobic floors are selective to a dominant HMM configuration with actin-binding sites. (F) Selective attachment and motility of actin filaments in the network channels and no attachment is observed on the polymer surfaces and walls.

3.2 Surface functionalization

For the *in-vitro* motility assay (IVMA) assay, the configuration of the HMM motors needs to be different on the channel floors and the resist walls to provide selective movement of filaments inside the channels, while ideally blocking movement anywhere else. HMM configuration supports actin motility when adsorbed on hydrophobic surfaces with high contact angles in the range of 75-81 degrees and the configuration of HMM exhibits no binding sites for actin when adsorbed on hydrophilic surfaces with low contact angles[71,72]. This selectivity in the prepared devices is obtained by ashing the developed chips with oxygen plasma at 5 mbar for 45 s to make the resist walls hydrophilic thereby not supporting the actin attachment and activating the exposed SiO_2 channel floors by exposing hydroxyl groups which would then react with silane to make the surface hydrophobic[73] as depicted in Figure 3.1 E. The samples were silanized with trimethylchlorosilane (TMCS), a silane proven to result in high actin motility[71], in a controlled chamber at 200 mbar to get the desired surface chemistry with high contact angle for adsorption of HMM onto the exposed SiO_2 surfaces supporting actin motility[72], as seen in Figure 3.1 F.

3.2.1 In-vitro motility assay

IVMAs are widely used to study the properties of molecular motor systems[19,74]. The IVMA used in our experiments with actin-myosin system is called the gliding assay[75]. Here, the cytoskeletal filaments are fluorescently labelled and are propelled by the non-labelled HMM. The HMM which is adsorbed to the substrate forms the dominant region with heads that is primary for motor function.

To conduct IVMAs, NBC devices are assembled in flow cells and chips are affixed to microscopic coverslips with stretched parafilm. The assay is performed by capillary force, where various assay solutions are flowed through the chips as illustrated in Figure 3.2 A. Using a fluorescent microscope, the movement of fluorescently labelled filaments is recorded, as shown in Figure 3.2 B. These time-lapse images are then analyzed to gather information on the paths taken by filaments in the network.

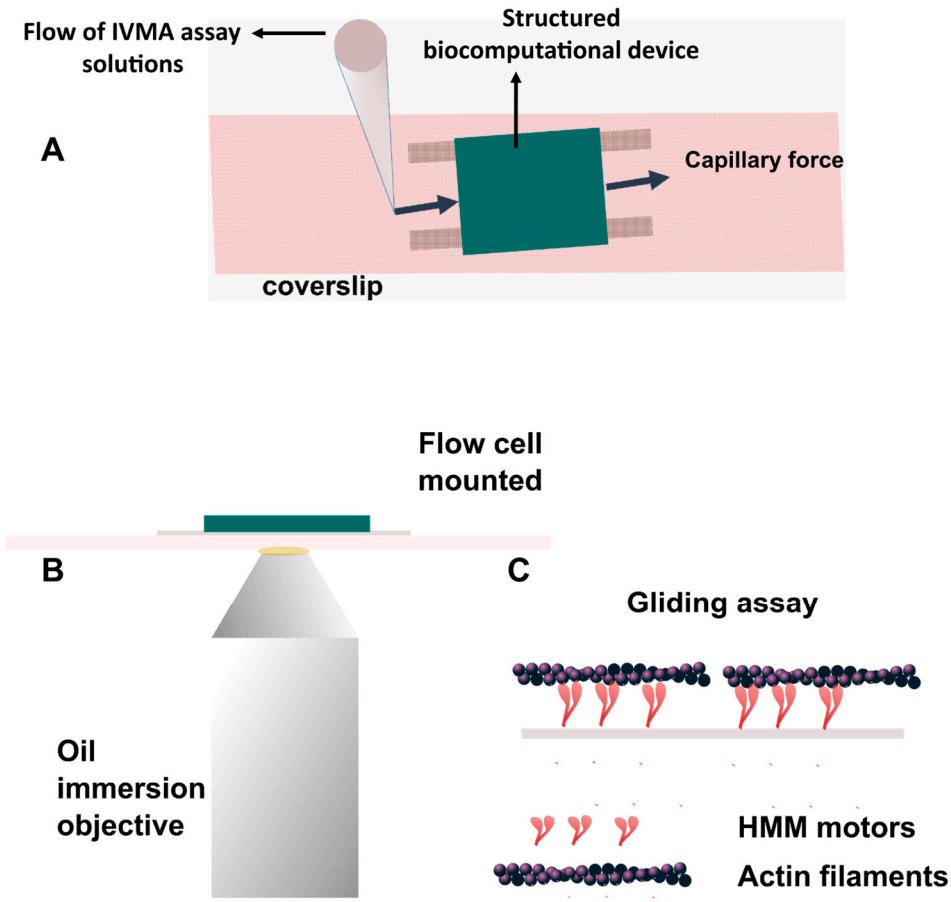

Figure 3.2: Schematic of the IVMA process (A) Flow cell prepared for the IVMA assay with the structured sample mounted on the parafilm spacers such that the assay solutions enter the structure through capillary force. (B) An oil immersion objective was used to observe the movement of the actin filaments from the bottom. The coverslip is thin enough to capture the motility of the structures. (C) The gliding assay uses adsorbed HMM motors to propel the fluorescently labeled actin filaments across a surface.

3.3 Effect of process parameters on motility (Paper I)

For over a decade, we have employed the aforementioned methods to develop nanodevices utilized in NBC. However, a consistent observation has been inadequate attachment and motility of filaments within these nanodevices. As discussed in section 3.1 and 3.2, several process parameters are essential for achieving an effective device with optimal performance. Even minor modifications to any of the process parameters can influence motility. Unfortunately, due to practical considerations, numerous changes occur over time, encompassing the utilization of new material batches for chemicals such as resists and silane, modifications in equipment like electron-beam lithography (EBL) that undergo routine enhancements and maintenance, and other practical alterations. A systematic approach is therefore required to re-establish the surface quality of the nanodevices by benchmarking the process parameters. Three regions of the networks: loading zones (Figure 3.3 a), nanochannel (Figure 3.3 b), and microchannel (Figure 3.3 c) were tested for HMM motor adsorption by fluorescent labelling of the HMMs. We observed regions of non-uniform HMM adsorption which can affect the actin motility and attachment, showing the significance of optimizing process parameters.

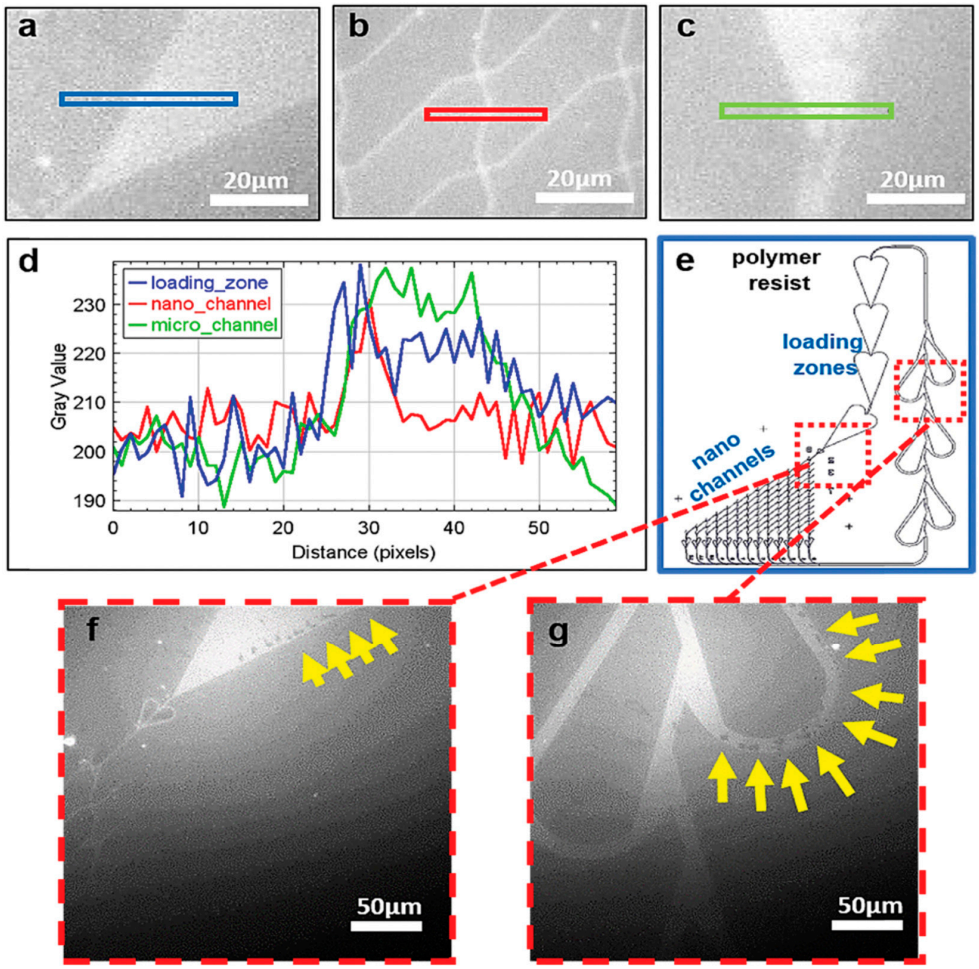

Figure 3.3: Fluorescently labeled HMM on different parts of the NBC device. Adapted from Paper I, Copyright (2021) IOP Publishing under license CC BY 4.0 (open access).

The ensuing factors have been examined for improving performance (detailed in Paper I):

- **SiO_2 Substrates:** We conducted tests using two kinds of substrates: one with an oxide layer created through Atomic Layer Deposition (ALD), and the other with an oxide layer formed via thermal oxidation. We observed that the motility run times were comparable for both substrate types.
- **Resist for EBL:** Prior studies have investigated various types of resists for their biocompatibility and their impact on actin motility[72]. In our recent experiments, we have identified the CSAR62 resist as the most suitable option for actin

devices. While PMMA also yields comparable motility results, CSAR62 resist offers the advantage of significantly shorter EBL write times.

- **Polymer development after cross-linking:** Both amyl acetate and MIBK: IPA developers demonstrated similar motility without any discernible differences.
- **Dicing of developed devices:** Typically, the developed devices were diced after developing the wafer. However, we noticed the presence of debris on the channel floors even after subjecting the structures to plasma ashing, indicating the inorganic nature of the debris, as depicted in Figure 3.4. This debris could potentially originate from equipment and the cooling water spray during the dicing process. In contrast, when dicing was performed before development, the resist layer served as a protective barrier, resulting in the absence of debris after plasma ashing, as illustrated in Figure 3.4(d).

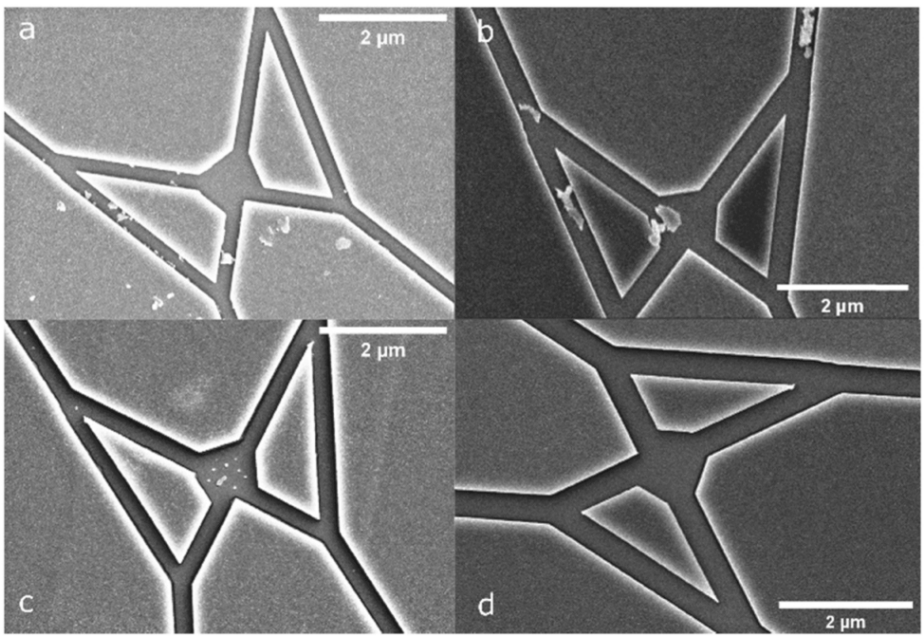

Figure 3.4: SEM images of the devices (a) Dicing after the development of devices (b) Same device in (a) after plasma ashing (c) Dicing before the development of devices (d) Same device in (c) after plasma ashing. Adapted from Paper I, Copyright (2021) IOP Publishing under license CC BY 4.0 (open access).

Plasma etching and TMCS silanization: One of the most crucial steps for ensuring the prolonged motility of devices is the plasma treatment and TMCS silanization, responsible for establishing the right surface chemistry conducive to selective and guided motility[76]. As depicted in Figure 3.3, non-uniform HMM adsorption was observed, which may be attributed to non-uniform silanization within the channels. To investigate the effects, etching and silanization times were varied between 15 to

45 s and 30 to 90 minutes, respectively. The results obtained indicated that the longest etching and silanization times (15 seconds and 90 minutes, respectively) exhibited the most favourable actin motility. However, the improvement in motility was only observed in the loading zones, and not in the narrower channels (100-200 nm). Subsequent investigations focused on two types of etching were done: anisotropic etching and isotropic etching.

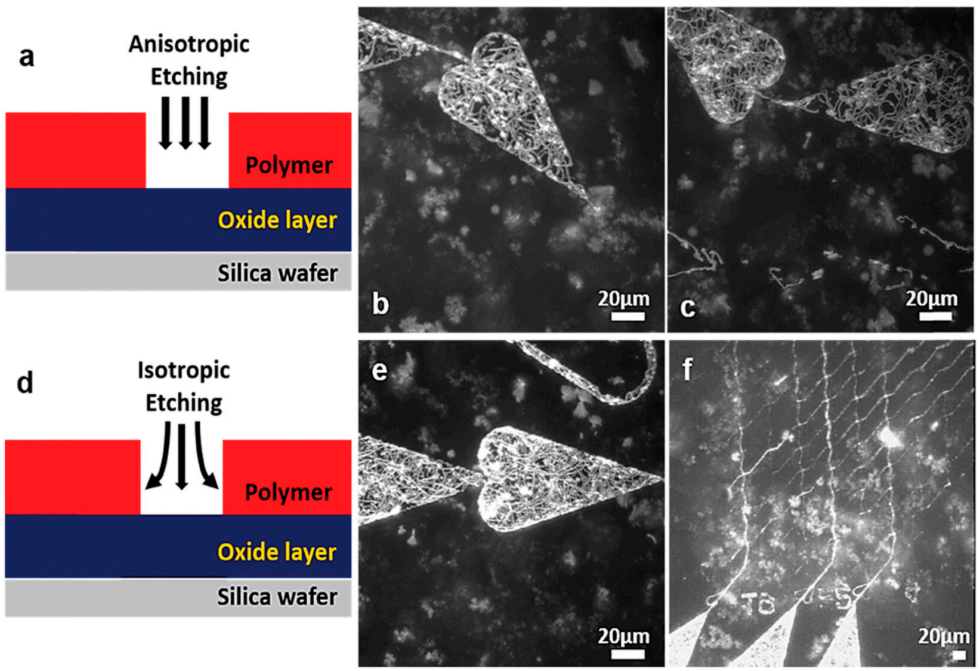

Figure 3.5: Comparison between isotropic and anisotropic etching of nano channels in the biocomputation network (a) Anisotropic plasma etching treats the target surface in a unidirectional manner. (b) and (c) Nanodevices exhibit motility in loading zones but not in nano-channels in result of anisotropic etching, despite the use of long (optimized) etching and silanization times. (d) Isotropic plasma etching treats the target surface in a more distributed manner, reaching the deep edges and walls in the nano channels. (e) and (f) Nanodevices show improved motility both in loading zones and nano channels following isotropic etching. Adapted from Paper I, Copyright (2021) IOP Publishing under license CC BY 4.0 (open access).

The anisotropic etching only led to higher etching rates at the channel floors compared to that of the sidewalls. This meant that the HMM was adsorbed in undesirable configurations, resulting in poor motility in narrow channels, as illustrated in Figure 3.5. On the other hand, isotropic etching resulted in uniform etching on both the bottom and sidewalls. The motility of actin filaments was tested in both cases, revealing good motility in both the loading zones and the narrow channels, as depicted in Figure 3.5(f). The optimization of all these conditions

extended the motility run times to > 60 minutes, as demonstrated by measurements of the sliding velocity and number of motile filaments in Figure 3.6.

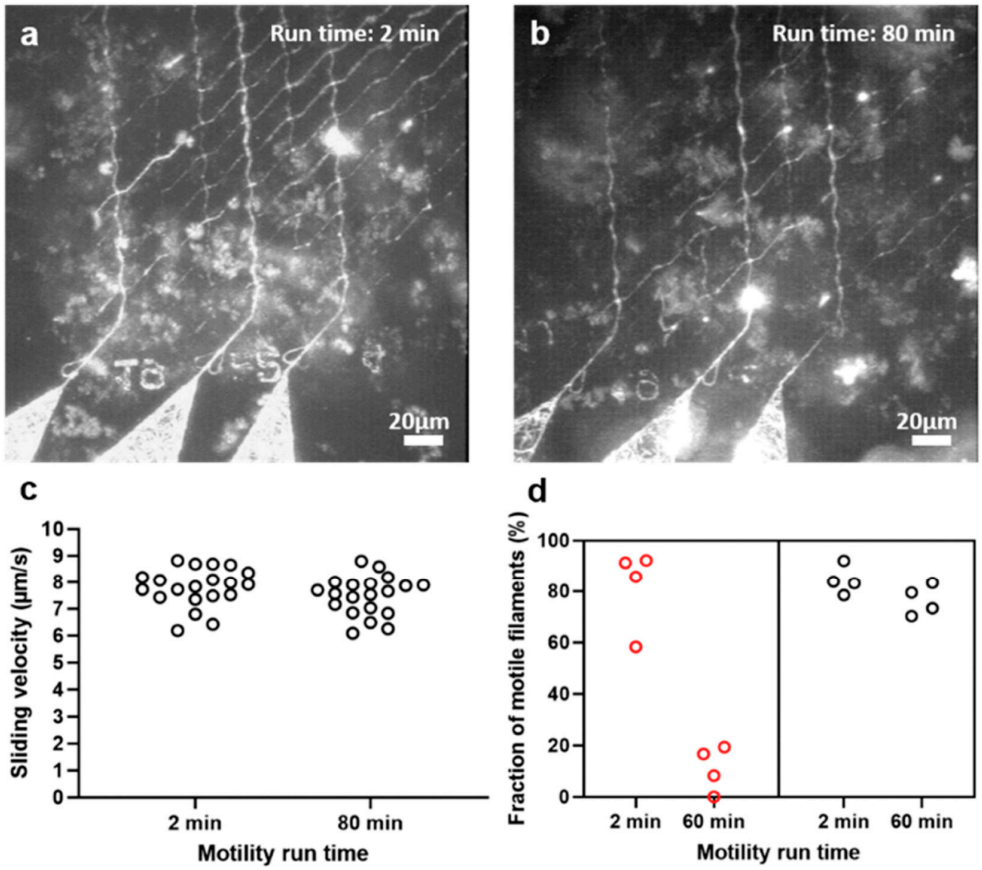

Figure 3.6: Analysis of motility in the biocomputation network under fully optimized conditions, including isotropic etching. (a) the motility of actin–myosin at 2 minutes. (b) the function of actin-myosin at 80 minutes. (c) sliding velocity in the nano channels remains consistent after 80 minutes of run time (d) the fraction of motile filaments before optimizations (in red) and after applied optimizations (in black) under the same temperature conditions. Images (a) and (b) are generated as maximum projection stacks of 100 frames acquired 2 minutes and 80 minutes after the start of the assay, respectively. In (c), 20 filaments were analyzed for each time point in the nano channel networks shown in (a) and (b). In (d), four loading zones were examined, distributed over four different experimental occasions. Adapted from Paper I, Copyright (2021) IOP Publishing under license CC BY 4.0 (open access).

4. Solving Exact Cover and SAT using actin-myosin based NBC

We describe the method of conversion of ExCov into an SSP network using the developed algorithm and the experimental solving of an ExCov instance using the actin-myosin system and the analysis of error rates. We also describe the experimental results for the solving of 3-SAT instances using NBC.

4.1 Solving Exact Cover using actin-myosin based NBC (Paper II)

In Paper II, two instances of 5-set ExCov problem named as $E32_1$ and $E32_0$ were experimentally solved. The instance $E32_1$ is chosen such that it has a solution whereas the instance $E32_0$ does not have a solution. An example is given here to illustrate an ExCov solution.

For a given target set, X = {1, 2, 3, 4,5}, and subsets, S = [{4, 5}, {2, 3, 5}, {1, 4}, {1, 3}, {1, 2}, the ExCov solution S = {(2,3,5), (1,4)} whereas a subcollection S'={(1,3), (1,4)} will not be a solution as 1 is repeating and 2 and 5 are missing.*

An optimized network encoding algorithm of ExCov problem to solve by NBC was developed by our collaborators[77]. This algorithm works by converting the ExCov problem into a SSP network (see section 2.3.2), briefly described by the following steps.

- The elements of the given target set X and the subsets from S are mapped to bits of a binary number. This is done by setting bit '1' to the elements of the target set present in the given subset and '0' is set to the elements of the target set not present in the subset.
- Then the decimal numbers form the new set of numbers which are used to design the SSP network. Table 4.1 depicts the steps used. The ExCov solution of the problem has 1 in all the bit locations as it has all the elements of the target set X and thus the sum corresponding to this is the required solution. Thus, in the network, we only need to look at the exit corresponding to the target solution

and if a significant number of filaments exits at this network exit, then the sub-collection of sets contains an exact cover. If an instance of the ExCov problem does not have a solution, then the agents do not arrive at the solution exit. In the given example, 31 is the solution exit.

Table 4.1. Network encoding algorithm for the given ExCov instance

	Set	Binary number	Conversion of the binary number	Decimal number
Set 1	(4,5)	0 0 0 1 1	2^1+2^0	3
Set 2	(2,3,5)	0 1 1 0 1	$2^3+2^2+2^0$	13
Set 3	(1,4)	1 0 0 1 0	2^4+2^1	18
Set 4	(1,3)	1 0 1 0 0	2^4+2^2	20
Set 5	(1,2)	1 1 0 0 0	2^4+2^3	24
Exact cover	(1,2,3,4,5)	1 1 1 1 1	$2^4+2^3+2^2+2^1+2^0$	31

4.1.1 Experimental results

Based on the network encoding algorithm, instance $E32_1$ and instance $E32_0$ were designed (as shown in Figure 4.1). The target set and the subset values corresponding to the instances are described in the Figure 4.1. The binary conversion of the instances is also shown. The filaments should exit at column 31 for the ExCov instance with solution, $E32_1$ whereas for instance $E32_0$ which has no solution, no filaments should exit from column 31.

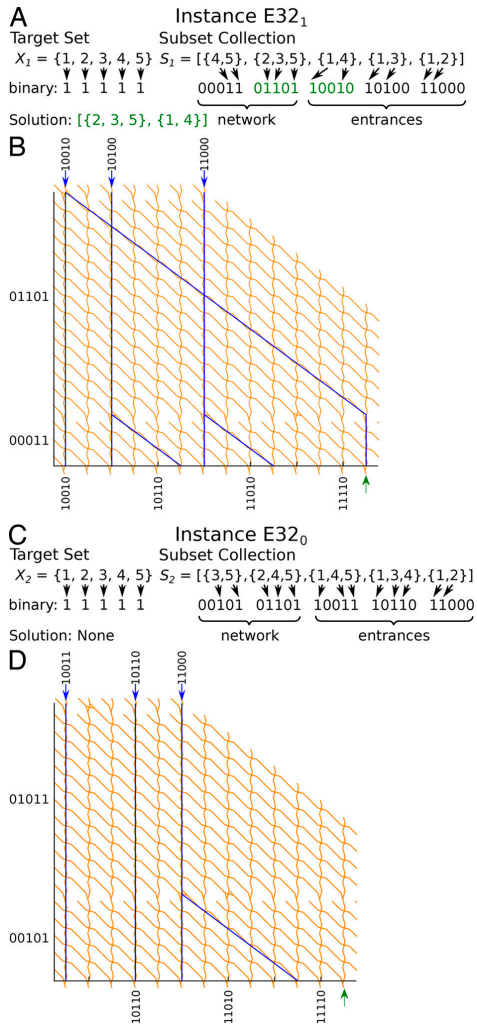

Figure 4.1: Five-set Exact Cover instances transformed into network format. (A, C) Instance $E32_1$ (A) and Instance $E32_0$ (B) with binary mappings of target sets X1 and X2, along with subsets in S1 and S2 as detailed in Table 4.1. (B, D) networks encoding Instance $E32_1$ (B) and Instance $E32_0$ (D), enabling agents exploring the network to randomly choose subcollection of sets from S1 or S2 according to Exact Cover rules outlined in Table 4.1. The solution to the Exact Cover instance encoded by the network can be determined by checking if agents exit at the binary representation of the target set (green arrows in (B) and (D)). If a substantial number of agents reach that specific exit, then the Exact Cover instance has a solution; otherwise, it does not. (A, B) Represent an Exact Cover instance with a solution. (C, D) Represent an Exact Cover instance without a solution. (B, D) Blue arrows denote network entrances; correct paths are highlighted in blue. Adapted from Paper II, Copyright (2022) ACS Nanoscience Au under license CC BY 4.0 (open access).

In our network, there are three types of junctions to modulate the motion of filaments in the channel network: (i) pass junctions (ii) split junctions. (iii) reset junctions. The pass and split junctions have been used earlier in the network solving SSP[17] (described in Chapter 2). Reset junctions[77] are introduced in place of split junctions where identical elements of subsets cannot be combined as it can create false-positive solutions (details in Paper II). The device fabrication and data collection were done as described in Chapter 3. Time-lapse fluorescent images of the movement of fluorescently labelled filaments in the network was recorded. The number of filaments coming out of all the exits including the target exit 31 corresponding to (1,1,1,1) was counted. Figure 4.2 (A) and (C) show the standard deviation plots of the time-lapsed superimposed fluorescent images where the frequently visited paths are brighter than the rest of the network highlighting the path of the filaments.

The performance of the pass junction significantly influences the error rates and overall device performance. Filaments that move straight through the pass junction are considered to have taken the correct turns. In contrast, those who make a turn are regarded as having taken incorrect paths, resulting in erroneous counts (Figure 2.2). The junction error rate E is calculated as the number of incorrect filaments at a junction divided by the total number of passing filaments, N. For instances, $E32_1$ and $E32_0$, E was found to be ~3.8% and ~2.6% error, respectively. Furthermore, the filaments that arrived at each exit were counted. Based on the error rates and the total number of filaments, threshold values were calculated for correct and incorrect counts (details in the SI section S1 of paper II). For the instance $E32_1$, more filaments exited at 31 more than the correct threshold value, indicating an exact cover solution. In contrast, for instance, $E32_0$, the number of filaments exiting at the target exit was very low than the incorrect threshold value, indicating no solution as expected (shown in Figure 4.2). The results demonstrated the successful solving of ExCov problems using NBC. However, the error rates obtained in our experiments were high which should be reduced to further scale up NBC. Error mitigation strategies are discussed in Chapter 5.

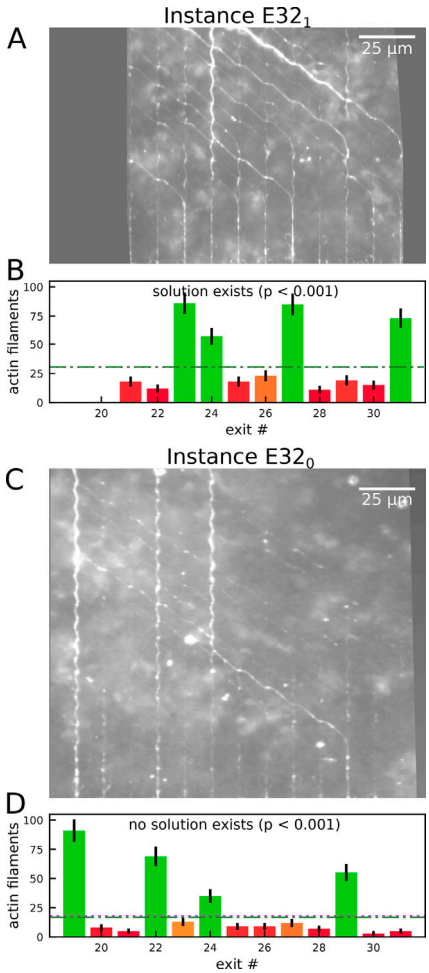

Figure 4.2: Successful operation of optimized Exact Cover networks with 5 sets (32 potential solutions) using the actin-myosin system. Optimized networks encoding Exact Cover instances $E32_1$ (A, B) and $E32_0$ (C, D). (A, C) Show standard deviation projections of 2500 frames from 0.2-second time-lapse fluorescence micrographs of computing networks. Brighter paths are the ones more frequently traversed by actin filaments (B, D) Display the number of actin filaments counted at each exit. RGB colors indicate probabilities that the counts correspond to correct (more green) or incorrect (more red) exits. Error bars represent counting errors. Values above the green dash-dotted lines signify significantly correct exits while values below the magenta dotted lines signify significantly incorrect exits (see SI of paper II). The rightmost exit 31 correspond to solutions for the Exact Cover instances. Adapted from Paper II, Copyright (2022) ACS Nanoscience Au under license CC BY 4.0 (open access).

4.2 Solving 3-SAT using actin-myosin based NBC (Paper III)

In a recent study, the development of the NBC algorithm for solving another NP-complete problem, 3-SAT was experimentally demonstrated[78]. The notations used and different components of SAT are explained in detail in section 2.1.3 of Chapter 2. The conditions to achieve satisfiable solution are also described. Four different instances of SAT were solved which were denoted by $\varphi_1, \varphi_2, \varphi_3$ and φ_4 as follows.

$$\varphi_1 = (x_1 \vee x_2) \wedge (\neg x_1 \vee x_2) \wedge (x_1 \vee \neg x_2) \wedge (\neg x_1 \vee x_2) \quad (4.1)$$

$$\varphi_2 = (x_1 \vee x_2) \wedge (\neg x_1 \vee x_2) \wedge (x_1 \vee \neg x_2) \wedge (\neg x_1 \vee \neg x_2) \quad (4.2)$$

$$\varphi_3 = (x_1 \vee x_2) \wedge (\neg x_1 \vee x_2) \wedge (x_1 \vee \neg x_2) \wedge (\neg x_1 \vee \neg x_2 \vee x_3) \wedge (x_1 \vee x_2 \vee x_3) \quad (4.3)$$

$$\varphi_4 = (x_1 \vee x_2) \wedge (\neg x_1 \vee x_2) \wedge (x_1 \vee \neg x_2) \wedge (\neg x_1 \vee \neg x_2) \wedge (x_1 \vee x_2 \vee x_3) \quad (4.4)$$

The instance φ_1 solves two variables and four clauses. It was chosen such that there is a satisfiable assignment. In addition, φ_2 (two variables, four clauses, and no solution), φ_3 (three variables, five clauses, and one solution) and φ_4 (three variables, five clauses, and no solution) were solved. The network algorithm was developed to convert SAT instances into NBC networks and was solved using actin-myosin system[78].

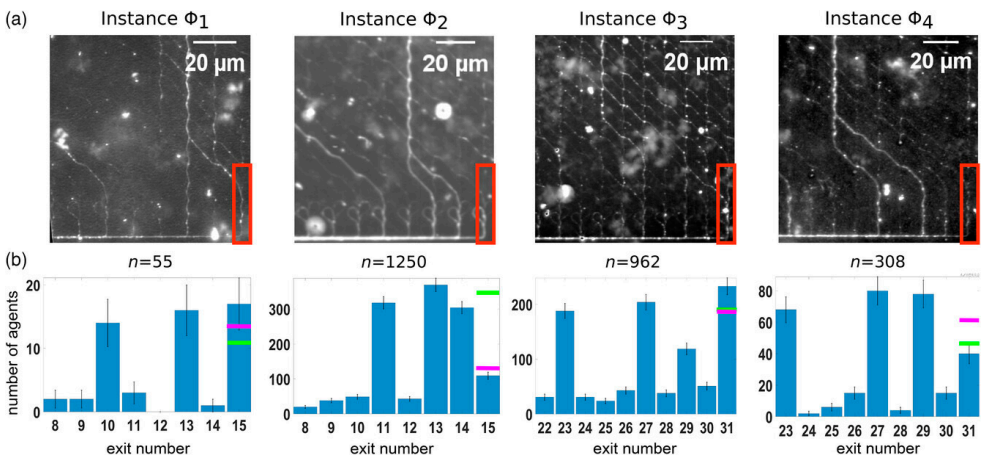

Figure 4.3: Experimental read-out for four instances of 3-SAT ($\varphi_1, \varphi_2, \varphi_3, \varphi_4$ (a) Standard deviation of projections from 1000 fluorescence images showing the movement of actin filaments through the device. (b) Shows experimental results obtained from manually counting actin filaments passing through the exits at the bottom. The total counted events (n) are displayed, with error bars representing the counting error. For the target column (15 for φ_1, φ_2, and 31 for φ_3, φ_4, as indicated by red boxes in (a)), values above the magenta bar indicate significantly correct exits (corresponding to a 99% confidence level, Supporting

Information 1[78]), while values below the green bar denote significantly incorrect exits (Supporting Information 1[78]). Adapted from Paper III, Copyright (2022) Wiley Online Library under license CC BY 4.0 (open access).

Based on the developed algorithm, the exits corresponding to satisfiability for all the four instances was found (details in paper III). The instances φ_1 and φ_2 had 16 exits (0-15) with exit 15 corresponding to satisfiability. Similarly, the instances φ_3 and φ_4 had 32 exits (0-31) with exit 31 corresponding to satisfiability. In this thesis work, the experimental demonstration of solving these instances was carried out by using the methods described in Chapter 3. The results showed that the instances φ_1 and φ_3 were satisfiable indicated by the high number of filaments exiting at the target exits as shown in Figure 4.3. In contrast, the instances φ_2 and φ_4 were unsatisfiable as the number of filaments in the target exits is below the calculated threshold. All the instances were solved with a 99% confidence interval.

5. Error propagation for scaling-up NBC

To address the challenges of error rates in the pass junction when solving combinatorial problems using NBC, two solutions are proposed in this chapter. The first solution involved optimizing current 2D junctions by identifying key geometry parameters, while the second solution involved creating 3D junctions for complete error prevention.

5.1 2D pass junction geometry optimization (Paper IV)

For the future development of NBC technology, focusing on scaling up and improving performance, reducing error rates is a crucial step[24,25]. In previous studies, the pass-junction error rates for actin-myosin-based devices were found to be in range between 2-4%[1,17]. In this work, we aimed to further minimize error rates within the current 2D networks by optimizing the pass junction geometry. The key parameters were identified and systematically varied them as part of the optimization process. The persistence length (L_p) of actin filaments of 10 μm[79], which determines their bending stiffness, is a crucial factor considered while designing the pass junctions. Due to that, the channel widths need to be less than 200 nm to prevent filaments from making U-turns within the channels[80,81].

Previous research has demonstrated that filaments travel along the channels' bottom wall as they enter the incoming channels[82]. This behaviour increases the risk of filaments hitting the junction outgoing channel corner instead of smoothly transitioning along the outgoing channels. Therefore, we introduced an offset (as shown in Figure 5.1) to the outgoing channels to address this issue. To further enhance filament guidance in the junction area, we considered the inclusion of funnels as an additional component within the junction which proved to be useful earlier[1,17]. The angle at which these funnels are positioned can also impact their effectiveness in guiding filaments within the junctions. In summary, based on our observations, the key geometry parameters (as shown in Figure 5.1) that can influence pass junction errors include:

- Channel width, C (0-200 nm)
- Offset distance, O (0-45 nm)
- Funnel width, F (0-110 nm)
- Funnel angles, α and β (0-45 degrees)

Sixteen designs were developed by varying these junction parameters (details in Figure 2 and Table 1 of Paper IV). The channels in the junction are symmetric. These designs' error rates were evaluated using a small (2,3) SSP network (Figure 1 of paper IV).

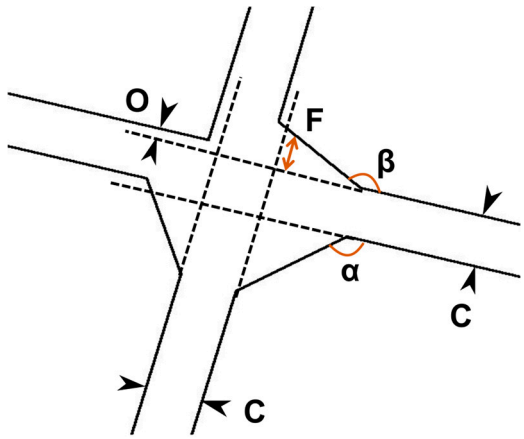

Figure 5.1: Schematic of the junction geometry and its parameters. Adapted from Paper IV (manuscript).

The fabrication process of the devices is detailed in the Chapter 3. The data collection and error rates calculation are described in section 4.1.1. Error rate, E were calculated as the ratio of the total number of incorrect filaments to the total number of filaments. The measured error rates are displayed in Figure 5.2 (orange colour bars). The F_{110} design (C= 100 nm, O = 22 nm, F= 110 nm, α= 45° and β=45°) exhibited the lowest error rate of 0.9%. Designs with narrower channel widths, shorter offset distances, and wider funnels demonstrated better performance with reduced error rates.

5.1.1 Comparison of simulation and experimental error rates

In Paper IV, we also utilized a simulation approach developed from previous works[82]. In this simulation, the filament tip is modelled as a point within a channel, considering a specific persistence length as they navigate through confined regions

of motility. The software monitors the time steps taken by the filaments, corresponding to an L_p value of 10 µm. Another parameter called edgestickiness (ES) was also used in the simulation which corresponds to the probability of filaments getting stuck and turning around. The code produces heatmaps, movies, and error rate information related to filament movement for each design, which we employ as the surface (details provided in Paper IV).

In order to compare the experimental and simulation results, the simulation's error rates were analyzed and compared to the experimental error rates. Previous studies have shown that HMM can create a dense layer of >25 nm on both the channel walls and bottom[82]. To address this in our simulation model, we made the assumption that filaments entering the junction through an incoming entrance with their full length cannot breach the HMM layer on the channel walls at that entrance. This consequently reduces the effective channel width in which the filaments can move within that channel. However, they can penetrate the HMM layer in the other three outgoing channels, as they enter (or hit the HMM wall layer) with their leading tip as depicted in Figure 5.2. Consequently, simulations were conducted with two types of designs:

(A) the original design geometry

(B) a modified design geometry where one of the entrance channel widths was reduced considering HMM layer on the walls based on our assumption (as shown in the inset of Figure 5.3 B)

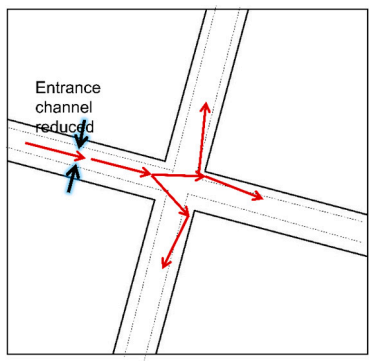

Figure 5.2. Movement of the filaments is represented by red arrows. The leading tip enters the junction and penetrates the outgoing channels. The black arrows show the entrance channels reduced to the width of the HMM layer, represented by the dotted lines. Adapted from Paper IV (manuscript).

We conducted simulations to explore the impact of varying HMM layers (ranging from 25-35 nm) and edgestickiness (ranging from 0 to 0.16). By utilizing the Bland-Altman plot[83,84], we identified the simulation parameters that yielded results most

closely resembling the actual experiments. The Bland-Altman plot, a graphical analysis used to analyse the fit between two methods, compares the mean error rates obtained from experiments and simulations and highlights their differences. In Figure 5.3, we compare the two designs we considered. As observed from the results, the modified design (B) gave better overall results than the original design (A). For design (B) the data points are tightly clustered around the mean line, indicating a strong correlation between the error rates observed from both methods. The mean value is nearly indistinguishable from zero, thus validating our hypothesis that filament can penetrate the HMM layer in the outgoing channels, not the channel it enters. On the other hand, for the original design (A), the mean is distinguishable (higher) from zero, and the data points are more scattered, indicating a weaker correlation between the two methods. The results show the significance of including HMM layer of 25-30 nm to improve the simulation, which can be in future used to design pass junctions.

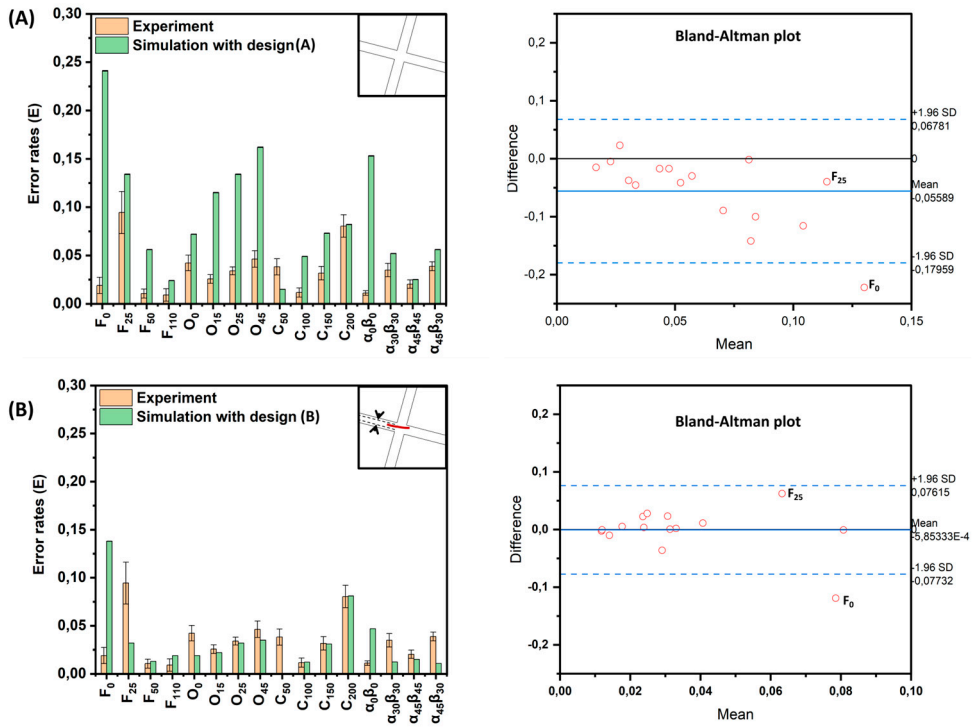

Figure 5.3: Comparison of experimental and simulation error rates using Bland-Altman plots (right). (A) Shows simulation results based on design geometries used in experiments, depicted in the inset. (B)

Illustrates simulation results with reduced width of incoming channels indicated by black arrows in the inset, accounting for the heavy meromyosin (HMM) layer (depicted by dashed lines in the inset). The penetration of filaments (highlighted in red in the inset) through the HMM layer in the outgoing channel from the junction is depicted, with a gliding direction from left to right. Error bars in the main panels represent counting errors. For these simulations, an HMM thickness of 30 nm and an ES of 0.12 were assumed. In the Bland–Altman plots, the X-axis shows the overall mean value of error rates measured by experiment and simulation, while the y-axis represents the difference of measured values. The solid blue line denotes the mean, and the dashed lines indicate the 95% upper and lower limits of agreement. Adapted from Paper IV (manuscript).

5.2 3D error-free junctions (Paper V)

2D junction optimization involved testing of all possible parameters and further error reduction in 2D junctions does not appear possible. This is due to the flexibility of the filaments which makes them turn around easily and due to the fabrication of the 2D geometry of the structures which can still result in incorrect turns of filaments. One of the possible solutions to further reduce computational error would be to develop a 3D junction with closed tunnels that would completely restrict the filaments' motility to the desired paths. This could be achieved by using a lithography technique called two-photon polymerization[85] based on commercial resist ORMOCER® as shown in Figure 5.4, developed by our collaborators. 3D structure with an overpass and an underpass (as shown in Figure 5.4) integrated into a 2D network could be an approach for error-free junctions in the future[86]. These types of error-free junctions were shown to be biocompatible[87], and desired fabrication resolution and channel roughness have been observed[85,86].

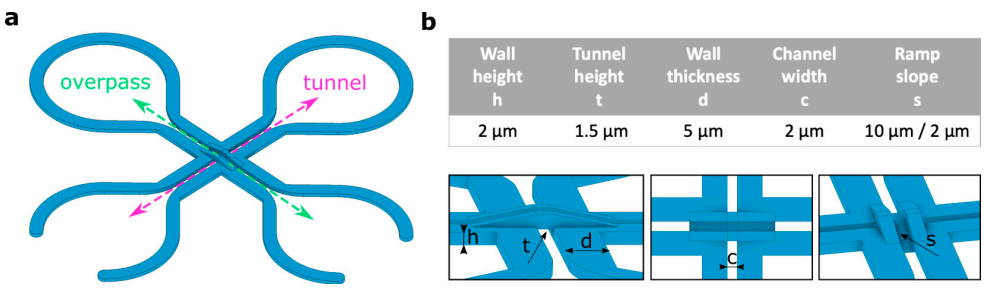

Figure 5.4: Design of 3D junction (a) 3D design of a junction featuring a tunnel and an overpass, each connecting a closed and an open reservoir. (b) Schematic images of the junction design (lower panel), with the corresponding parameters values (upper panel). Adapted from Paper V, Copyright (2021) IOP Publishing, under license CC BY 4.0 (open access).

The discussions in paper V focus on the microtubule-kinesin system[88]. Therefore, it was decided to test actin-myosin motility on proposed 3D ORMOCER® junctions. We conducted our first tests using silicon wafers that had been coated with various

planar ORMOCER® (OC) materials (including standard ORMOCER®, OC-I, and optical ORMOCER®, OC-V, two different chemically modified OCs). These surfaces were then subjected to different treatments (such as no treatment, plasma ashing, and plasma ashing with silanization). We measured water contact angles (WCAs) to determine the level of hydrophobicity present on each surface. These results can be found in Table 5.1.As it is known, efficient actin-myosin motility on surfaces is usually observed for WCAs in the range of 75-86 degrees on silicon wafers[71]. Therefore, the surface chemistry had to be tightly controlled to achieve uniform motor attachment for efficient motility. As a standard procedure, surfaces were cleaned with oxygen plasma to remove organic impurities, followed by silanization using trimethylchlorosilane (TMCS). WCAs within or close to the required range were achieved for OC- I after silanization with TMCS and OC-V without any surface treatment. Upon performing gliding motility assays for all surface conditions, we observed motility only on the OC-I with plasma treatment followed by TMCS silanization which had a desirable WCA range.

Table 5.1: Water contact angle (WCA) measurements and motility on planar OC-I and OC-V under different surface treatment conditions

Samples	Before surface treatment	After Plasma ashing (PA)	After PA and TMCS silanization	Observed actin attachment and motility
Standard OC, OC-I	85±2 °	Complete wetting of the surface	90±2 °	Motility observed on the surface before treatment
Optical OC, OC- V	88±2°	Complete wetting of the surface	99±2 °	Substrate was completely autofluorescent

However, OC-V showed high auto-fluorescence over the whole wavelength range of visible light, which made it unsuitable for motility experiments using fluorescence microscopy. 3D junction samples for actin-myosin testing were thus fabricated using OC-I with a design similar to what was used for the microtubule-kinesin system. These 3D junctions were treated with plasma and silanized with TMCS. During the motility assays, it was observed that only a few actin filaments were attached to the surface of the 3D-junction samples. Furthermore, there was no motility observed on either the structure or the surrounding surface, as illustrated in Figure 5.5. These observations of no motility on the 3D junction samples were in contradiction to our earlier results on planar standard OC samples. Given the surface treatment procedure was carried out in the same way, the surface chemistry of 3D junction OC samples may not be comparable directly to the planar OC surfaces. In future efforts, 3D junction samples thus need to be optimized separately for myosin attachment to achieve reliable actin motility on both the OC structure and the

substrate surface. Another possible approach could be a design that allows actin motility only on the OC surface.

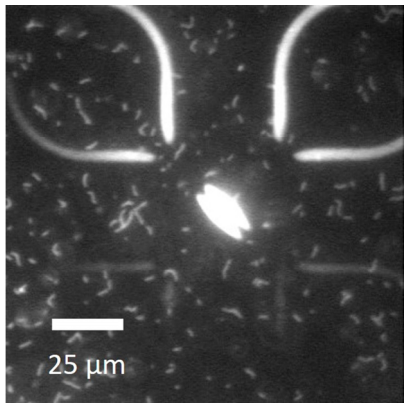

Figure 5.5: Standard deviation projection of 100 fluorescent images showing overpass and tunnel design with OC I, with very little actin attachment and no motility.

With this aim, a new 3D design was developed in which a simple overpass connects two loading zones made from OC whereas two other loading zones are connected by a straight channel (Figure 5.6 A). It was hypothesized that it might be easier to find suitable surface conditions and achieve the desired 3D motility of actin filaments. The successful demonstration of such 3D motility would enhance their potential use as error-free junctions in biocomputational devices.

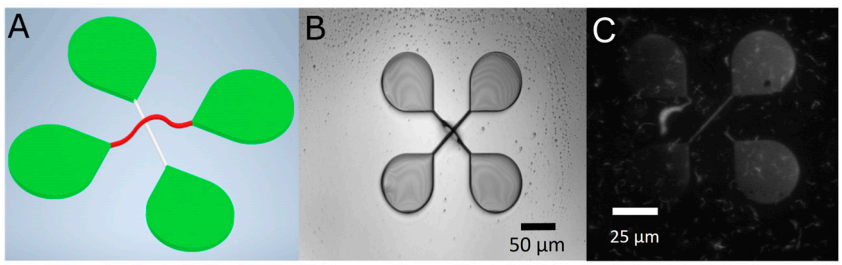

Figure 5.6: New simpler 3D design for actin-myosin system. (A) Schematic of overpass design for actin-myosin system, (B) Optical image of the structure fabricated by two-photon polymerization, (C) Standard deviation projection of 100 fluorescent images of the overpass structure with no actin attachment and motility

However, as depicted in Figure 5.6 C, it turned out to be challenging to generate an OC overpass that supports motility of satisfactory quality, while preventing motility on the rest of the planar substrate. Hence, more future optimization is needed for several parameters such as material, design, and surface chemistry to achieve the desired 3D junctions for the actin-myosin system.

6. Conclusions and Outlook

In this thesis, we have realized several requirements necessary to improve and expand the application of NBC technology. A significant accomplishment includes the standardization and optimization of nanodevice development for NBC. The performance of actin-myosin NBC devices was enhanced, increasing their operational run-time from < 20 minutes to over 60 minutes (Paper I). Our research shows that the NBC approach can solve Exact cover problems that are four times larger in scale than those previously solved by the actin-myosin system used for SSP, as outlined in Paper II. This experimental finding indicates that the NBC approach is highly adaptable and capable of addressing more significant problem instances. Additionally, we have successfully executed the first experimental demonstration of the NBC algorithm for the Satisfiability problem in Paper III.

However, there are limitations to scaling up these devices, such as error rates in the pass junctions. We have made significant progress in optimizing the 2D pass junction geometry for actin-myosin based devices by utilizing experimental and simulation approaches, by achieving an error rate of less than 1%, as explained in Paper IV. While this is a crucial step towards scaling up to devices with hundreds of pass junctions, our exhaustive approach has also revealed the need for other methods to eliminate error rates. One solution is 3D junctions with tunnels and passes fabricated using two-photon polymerization. This approach has the potential to develop error-free junctions, as described in Paper V. Furthermore, we have conducted a preliminary evaluation of the materials, material design, and surface chemistry required for the actin-myosin system.

To attain a level of performance in NBC comparable to electronic computing, there are still several requirements that must be addressed. Below are some of these requirements along with potential solutions.

Large-scale production of nanodevices: The current technology of EBL is limited by the time taken for fabrication and cost inefficiency as the device size increases. In the future, it is possible to use other state-of-the-art lithography techniques such as nanoimprint lithography (NIL) which is cost-efficient with high throughput within a short span of time compared to EBL[89]. NIL can be used to create multiple identical networks with desired resolution, allowing for parallel operation of devices necessary for data collection.

Devices for filament multiplication: Self-replicating filaments are crucial for increasing the feeding rate in the devices because the need for agents increases with the increase in the problem size[25]. The protocol for elongation and multiplication of the actin filaments has been optimized on planar surfaces by our collaborators from Linnaeus university, Kalmar. For using the developed methods of filament splitting and elongation in biocomputational devices, it becomes vital to optimize their movement on lithographically fabricated devices. The initial experiments would be to transfer the protocol to micropatterned SiO_2 surfaces such as flower structures in Figure 6.1A. This is necessary to understand the behavior of split filaments on the processed substrates before moving to narrow patterned channels that are used in NBC. A loop design with nanochannels depicted in Figure 6.1B with dimensions like the NBC devices is proposed for testing the filament multiplication. This design was shown to provide suitable unidirectional actin guidance for high-throughput assays and for studying the actin behavior as the filaments are trapped within the network[80].

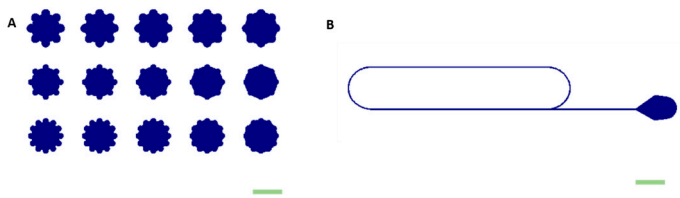

Figure 6.1: (A) Schematic layout for flower structures. The scale bar is 100 µm. (B) Schematic layout of nanostructured loop design. The scale bar is 1µm.

Integrated nanofluidic devices: When the NBC devices are scaled-up, we discussed the increased requirement for computing filaments. With the increase in the number of filaments, there is a need for a continuous supply of assay solutions for running the devices. This becomes a decisive factor for operating the devices for a long time. This is vital in terms of getting sufficient data on the track of filaments, which is a crucial factor for the error rates. One possibility to address this problem in the future would be to integrate our nanofabricated with microfluidic devices with multiple inlets as shown in Figure 6.2 which could provide the continuous flow of the solutions needed for filament motility[90,91]. The recent development in the field of microfluidic and nanofluidic devices imparts advantages of controlled depth of patterns, multi-level 3D structures lending flows to different parts of the devices, and reliable sealing of the devices[91–93]. In addition, these devices are valuable tools for single molecule detection[93–95]. This can be proficiently used in NBC devices for the detection of our filaments as an alternative to the currently used optical detection method of fluorescence microscopy.

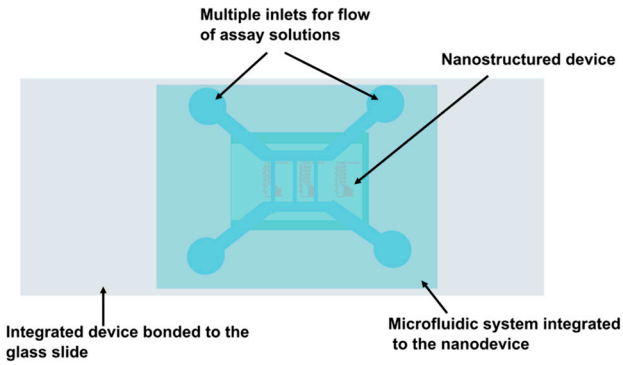

Figure 6.2: Schematic of integration of the nanostructured device with a microfluidic system for continuous supply of assay solutions

Towards other applications of our technology: In the field of molecular biology and protein engineering, the diffusion of proteins and other biomolecules is of great importance to understand their behavior. Some of the recently developed synthetic artificial molecular motors[96] are inspired by motor proteins with directed motion. The characterization of such developed motors can impart knowledge on the fundamental biophysical properties of motor proteins[97]. In our devices, we used a combination of physical patterning and chemical modification for the directed motion of the cytoskeletal filaments across the surface. This results in controlled 1D diffusion of filaments in the nanochannels. Hence, our selective directed motility technology can be harnessed to study the diffusion of the developed artificial molecular motors as shown in Figure 6.3 to understand the underlying phenomenon[96,98] and for other nanotechnological applications[99].

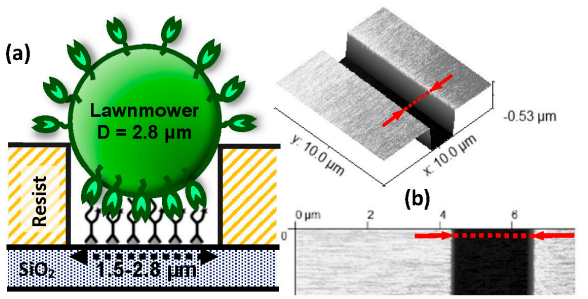

Figure 6.3: Microchannels designed for directing artificial molecular motor. (a) Cross-sectional schematic illustrating the interaction of artificial molecular motor within a channel, (b) AFM image depicting a portion of a fabricated channel. Adapted from Ref[96]. Copyright 2023 American Chemical Society under license CC BY 4.0 (open access).

References

(1) Surendiran, P.; Meinecke, C. R.; Salhotra, A.; Heldt, G.; Zhu, J.; Månsson, A.; Diez, S.; Reuter, D.; Kugler, H.; Linke, H.; Korten, T. Solving Exact Cover Instances with Molecular-Motor-Powered Network-Based Biocomputation. *ACS Nanosci. Au* **2022**, *2* (5), 396–403. https://doi.org/10.1021/acsnanoscienceau.2c00013.

(2) Wilson, L. International Technology Roadmap for Semiconductors (ITRS). *Semicond. Ind. Assoc.* **2013**, *1*.

(3) Arden, W.; Brillouët, M.; Cogez, P.; Graef, M.; Huizing, B.; Mahnkopf, R. "More-than-Moore" White Paper; More than Moore White Paper by the IRC, 2015. http://www.itrs2.net/uploads/4/9/7/7/49775221/irc-itrs-mtm-v2_3.pdf (accessed Apr. 11, 2016), 2010.

(4) Konopik, M.; Korten, T.; Lutz, E.; Linke, H. Fundamental Energy Cost of Finite-Time Parallelizable Computing. *Nat. Commun.* **2023**, *14* (1), 447. https://doi.org/10.1038/s41467-023-36020-2.

(5) Mack, C. A. Fifty Years of Moore's Law. *IEEE Trans. Semicond. Manuf.* **2011**, *24* (2), 202–207.

(6) Garey, M. R.; Johnson, D. S. *Computers and intractability : a guide to the theory of NP - completeness*; W.H. Freeman and Co.: New York, 2003.

(7) Chabert, M.; Solnon, C. A Global Constraint for the Exact Cover Problem: Application to Conceptual Clustering. *J. Artif. Intell. Res.* **2020**, *67*, 509–547. https://doi.org/10.1613/jair.1.11870.

(8) Pierce, N. A.; Winfree, E. Protein Design Is NP-Hard. *Protein Eng. Des. Sel.* **2002**, *15* (10), 779–782. https://doi.org/10.1093/protein/15.10.779.

(9) Fraenkel, A. Complexity of Protein Folding. *Bull. Math. Biol.* **1993**, *55* (6), 1199–1210. https://doi.org/10.1016/s0092-8240(05)80170-3.

(10) Nicolau, D. V.; Nicolau Jr, D. V.; Solana, G.; Hanson, K. L.; Filipponi, L.; Wang, L.; Lee, A. P. Molecular Motors-Based Micro- and Nano-Biocomputation Devices. *Microelectron Eng* **2006**, *83* (4–9), 1582.

(11) Adleman, L. M. Molecular Computation of Solutions to Combinatorial Problems. *Science* **1994**, *266* (5187), 1021–1024. https://doi.org/10.1126/science.7973651.

(12) Boneh, D.; Dunworth, C.; Lipton, R. J.; Sgall, J. On the Computational Power of DNA. *Discrete Appl. Math.* **1996**, *71* (1–3), 79–94. https://doi.org/10.1016/s0166-218x(96)00058-3.

(13) Braich, R. S. Solution of a 20-Variable 3-SAT Problem on a DNA Computer. *Science* **2002**, *296* (5567), 499–502. https://doi.org/10.1126/science.1069528.

(14) Vandersypen, L. M. K.; Steffen, M.; Breyta, G.; Yannoni, C. S.; Sherwood, M. H.; Chuang, I. L. Experimental Realization of Shor's Quantum Factoring Algorithm Using Nuclear Magnetic Resonance. *Nature* **2001**, *414* (6866), 883–887. https://doi.org/10.1038/414883a.

(15) Xu, N.; Zhu, J.; Lu, D.; Zhou, X.; Peng, X.; Du, J. Quantum Factorization of 143 on a Dipolar-Coupling Nuclear Magnetic Resonance System. *Phys Rev Lett* **2012**, *108* (13), 130501. https://doi.org/10.1103/PhysRevLett.108.130501.

(16) Bengtsson, A.; Vikstål, P.; Warren, C.; Svensson, M.; Gu, X.; Kockum, A. F.; Krantz, P.; Križan, C.; Shiri, D.; Svensson, I.-M.; Tancredi, G.; Johansson, G.; Delsing, P.; Ferrini, G.; Bylander, J. Improved Success Probability with Greater Circuit Depth for the Quantum Approximate Optimization Algorithm. *Phys Rev Appl.* **2020**, *14* (3), 034010.

(17) Nicolau, D. V.; Lard, M.; Korten, T.; van Delft, F. C. M. J. M.; Persson, M.; Bengtsson, E.; Mansson, A.; Diez, S.; Linke, H.; Nicolau, D. V. Parallel Computation with Molecular-Motor-Propelled Agents in Nanofabricated Networks. *Proc Natl Acad Sci USA* **2016**, *113* (10), 2591.

(18) Hess, H. Engineering Applications of Biomolecular Motors. *Annu Rev Biomed Eng* **2011**, *13*, 429–450. https://doi.org/10.1146/annurev-bioeng-071910-124644.

(19) Howard, J. *Mechanics of Motor Proteins and the Cytoskeleton*; Sinauer Associates: Sunderland, Massschusetts., 2018.

(20) Piazzesi, G.; Lucii, L.; Lombardi, V. The Size and the Speed of the Working Stroke of Muscle Myosin and Its Dependence on the Force. *J. Physiol.* **2002**, *545* (1), 145–151. https://doi.org/10.1113/jphysiol.2002.028969.

(21) Hackney, D. D. Highly Processive Microtubule-Stimulated ATP Hydrolysis by Dimeric Kinesin Head Domains. *Nature* **1995**, *377* (6548), 448–450. https://doi.org/10.1038/377448a0.

(22) Uyeda, T. Q. P.; Kron, S. J.; Spudich, J. A. Myosin Step Size. *J. Mol. Biol.* **1990**, *214* (3), 699–710. https://doi.org/10.1016/0022-2836(90)90287-v.

(23) Van Delft, F. C. M. J. M.; Ipolitti, G.; Nicolau, D. V.; Sudalaiyadum Perumal, A.; Kašpar, O.; Kheireddine, S.; Wachsmann-Hogiu, S.; Nicolau, D. V. Something Has to Give: Scaling Combinatorial Computing by Biological Agents Exploring Physical Networks Encoding NP-Complete Problems. *Interface Focus* **2018**, *8* (6), 20180034. https://doi.org/10.1098/rsfs.2018.0034.

(24) Zhu, J.; Korten, T.; Kugler, H.; van Delft, F.; Mansson, A.; Reuter, D.; Diez, S.; Linke, H. Physical Requirements for Scaling up Network-Based Biocomputation. *New J Phys* **2021**, *23* (10), 105004.

(25) van Delft, F. C.; Månsson, A.; Kugler, H.; Korten, T.; Reuther, C.; Zhu, J.; Lyttleton, R.; Blaudeck, T.; Meinecke, C. R.; Reuter, D. Roadmap for Network-Based Biocomputation. *Nano Futur.* **2022**, *6* (3), 032002.

(26) Jones, N. D. Space-Bounded Reducibility among Combinatorial Problems. *J. Comput. Syst. Sci.* **1975**, *11* (1), 68–85. https://doi.org/10.1016/S0022-0000(75)80050-X.

(27) Cook, S. A. The Complexity of Theorem-Proving Procedures; ACM Press, 1971. https://doi.org/10.1145/800157.805047.

(28) Vikstål, P.; Grönkvist, M.; Svensson, M.; Andersson, M.; Johansson, G.; Ferrini, G. Applying the Quantum Approximate Optimization Algorithm to the Tail-Assignment Problem. *Phys Rev Appl.* **2020**, *14* (3), 034009.

(29) Ba, C. An Exact Cover-Based Approach for Service Composition; IEEE, 2016; pp 631–636.

(30) Impagliazzo, R.; Naor, M. Efficient Cryptographic Schemes Provably as Secure as Subset Sum. *J. Cryptol.* **1996**, *9* (4), 199–216. https://doi.org/10.1007/BF00189260.

(31) James, R. Methods for Solving Subset Sum Problems; 2003.

(32) James, R. J. W.; Storer, R. H. Techniques for Solving Subset Sum Problems within a given Tolerance. *Int. Trans. Oper. Res.* **2005**, *12* (4), 437–453. https://doi.org/10.1111/j.1475-3995.2005.00517.x.

(33) Oltean, M.; Muntean, O. Solving the Subset-Sum Problem with a Light-Based Device. *Nat. Comput.* **2009**, *8* (2), 321–331. https://doi.org/10.1007/s11047-007-9059-3.

(34) Knuth, D. E. Dancing Links. *ArXiv Prepr. Cs0011047* **2000**.

(35) Dehghan, M.; Seetharam, A.; Jiang, B.; He, T.; Salonidis, T.; Kurose, J.; Towsley, D.; Sitaraman, R. On the Complexity of Optimal Routing and Content Caching in Heterogeneous Networks; IEEE, 2015. https://doi.org/10.1109/infocom.2015.7218465.

(36) Shin, S.-Y.; Zhang, B.-T.; Jun, S.-S. Solving Traveling Salesman Problems Using Molecular Programming. In *Proceedings of the 1999 Congress on Evolutionary Computation-CEC99 (Cat. No. 99TH8406)*; 1999; Vol. 2, pp 994-1000 Vol. 2. https://doi.org/10.1109/CEC.1999.782531.

(37) Schoning, T. A Probabilistic Algorithm for K-SAT and Constraint Satisfaction Problems. In *40th Annual Symposium on Foundations of Computer Science (Cat. No.99CB37039)*; 1999; pp 410–414. https://doi.org/10.1109/SFFCS.1999.814612.

(38) Wu, X.; Wang, Z.; Wu, T.; Bao, X. Solving the Family Traveling Salesperson Problem in the Adleman–Lipton Model Based on DNA Computing. *IEEE Trans. NanoBioscience* **2022**, *21* (1), 75–85. https://doi.org/10.1109/TNB.2021.3109067.

(39) Hasudungan, R.; Pangestuty, D. M.; Latifah, A. J.; Rudiman. Solving Minimum Vertex Cover Problem Using DNA Computing. *J. Phys. Conf. Ser.* **2019**, *1361* (1), 012038. https://doi.org/10.1088/1742-6596/1361/1/012038.

(40) Qian, L.; Winfree, E. Scaling Up Digital Circuit Computation with DNA Strand Displacement Cascades. *Science* **2011**, *332* (6034), 1196–1201. https://doi.org/10.1126/science.1200520.

(41) Ouyang, Q. DNA Solution of the Maximal Clique Problem. *Science* **1997**, *278* (5337), 446–449. https://doi.org/10.1126/science.278.5337.446.

(42) Yin, Z.; Yang, J.; Zhang, Q.; Tang, Z.; Wang, G.; Zheng, Z. DNA Computing Model for Satisfiability Problem Based on Hybridization Chain Reaction. *Int. J. Pattern Recognit. Artif. Intell.* **2021**, *35* (3). https://doi.org/10.1142/S0218001421590102.

(43) International Workshop on, D. N. A. C.; Garzon, M.; Yan, H. DNA Computing : 13th International Meeting on DNA Computing, DNA13, Memphis, TN, USA, June 4-8, 2007 : Revised Selected Papers. **2008**.

(44) Ladd, T. D.; Jelezko, F.; Laflamme, R.; Nakamura, Y.; Monroe, C.; O'Brien, J. L. Quantum Computers. *Nature* **2010**, *464* (7285), 45–53. https://doi.org/10.1038/nature08812.

(45) Dash, A.; Sarmah, D.; Bikash; Prasanta. Exact Search Algorithm to Factorize Large Biprimes and a Triprime on IBM Quantum Computer. *ArXiv Pre-Print Serv.* **2018**.

(46) Martín-López, E.; Laing, A.; Lawson, T.; Alvarez, R.; Zhou, X.-Q.; O'Brien, J. L. Experimental Realization of Shor's Quantum Factoring Algorithm Using Qubit Recycling. *Nat. Photonics* **2012**, *6* (11), 773–776. https://doi.org/10.1038/nphoton.2012.259.

(47) Politi, A.; Matthews, J. C. F.; O'Brien, J. L. Shor's Quantum Factoring Algorithm on a Photonic Chip. *Science* **2009**, *325* (5945), 1221–1221. https://doi.org/10.1126/science.1173731.

(48) Dridi, R.; Alghassi, H. Prime Factorization Using Quantum Annealing and Computational Algebraic Geometry. *Sci. Rep.* **2017**, *7* (1), 43048. https://doi.org/10.1038/srep43048.

(49) Peng, X.; Liao, Z.; Xu, N.; Qin, G.; Zhou, X.; Suter, D.; Du, J. Quantum Adiabatic Algorithm for Factorization and Its Experimental Implementation. *Phys. Rev. Lett.* **2008**, *101* (22). https://doi.org/10.1103/physrevlett.101.220405.

(50) Gambetta, J. *IBM's roadmap for scaling quantum technology*. IBM Research Blog. https://research.ibm.com/blog/ibm-quantum-roadmap (accessed 2023-09-07).

(51) Huxley, H. E. Structural Difference between Resting and Rigor Muscle; Evidence from Intensity Changes in the Low-Angle Equatorial X-Ray Diagram. *J. Mol. Biol.* **1968**, *37* (3), 507–520. https://doi.org/10.1016/0022-2836(68)90118-6.

(52) Millman, B. M. The Filament Lattice of Striated Muscle. *Physiol. Rev.* **1998**, *78* (2), 359–391. https://doi.org/10.1152/physrev.1998.78.2.359.

(53) Ebashi, S.; Endo, M. Calcium and Muscle Contraction. *Prog. Biophys. Mol. Biol.* **1968**, *18*, 123–183. https://doi.org/10.1016/0079-6107(68)90023-0.

(54) Gordon, A. M.; Homsher, E.; Regnier, M. Regulation of Contraction in Striated Muscle. *Physiol. Rev.* **2000**, *80* (2), 853–924. https://doi.org/10.1152/physrev.2000.80.2.853.

(55) Rayment, I.; Holden, H. M. The Three-Dimensional Structure of a Molecular Motor. *Trends Biochem. Sci.* **1994**, *19* (3), 129–134. https://doi.org/10.1016/0968-0004(94)90206-2.

(56) Korten, T.; Mansson, A.; Diez, S. Towards the Application of Cytoskeletal Motor Proteins in Molecular Detection and Diagnostic Devices. *Curr Opin Biotechnol* **2010**, *21* (4), 477–488. https://doi.org/10.1016/j.copbio.2010.05.001.

(57) Holmes, K. C.; Popp, D.; Gebhard, W.; Kabsch, W. Atomic Model of the Actin Filament. *Nature* **1990**, *347* (6288), 44–49. https://doi.org/10.1038/347044a0.

(58) Gittes, F.; Mickey, B.; Nettleton, J.; Howard, J. Flexural Rigidity of Microtubules and Actin Filaments Measured from Thermal Fluctuations in Shape. *J. Cell Biol.* **1993**, *120* (4), 923–934. https://doi.org/10.1083/jcb.120.4.923.

(59) Månsson, A. Actomyosin-ADP States, Interhead Cooperativity, and the Force-Velocity Relation of Skeletal Muscle. *Biophys. J.* **2010**, *98* (7), 1237–1246. https://doi.org/10.1016/j.bpj.2009.12.4285.

(60) Winkelmann, D. A.; Baker, T. S.; Rayment, I. Three-Dimensional Structure of Myosin Subfragment-1 from Electron Microscopy of Sectioned Crystals. *J. Cell Biol.* **1991**, *114* (4), 701–713. https://doi.org/10.1083/jcb.114.4.701.

(61) Barclay, C. J. Estimation of Cross-Bridge Stiffness from Maximum Thermodynamic Efficiency. *J. Muscle Res. Cell Motil.* **1998**, *19* (8), 855–864. https://doi.org/10.1023/A:1005409708838.

(62) Kieke, M. C.; Titus, M. A. The Myosin Superfamily: An Overview. In *Molecular Motors*; 2002; pp 1–44. https://doi.org/10.1002/3527601503.ch1.

(63) Schliwa, M. *Molecular Motors*; Wiley-VCH: Weinheim, 2003.

(64) Kinesin Superfamily Proteins. In *Molecular Motors*; 2002; pp 79–109. https://doi.org/10.1002/3527601503.ch3.

(65) Kikumoto, M.; Kurachi, M.; Tosa, V.; Tashiro, H. Flexural Rigidity of Individual Microtubules Measured by a Buckling Force with Optical Traps. *Biophys. J.* **2006**, *90* (5), 1687–1696. https://doi.org/10.1529/biophysj.104.055483.

(66) Landauer, R. Irreversibility and Heat Generation in the Computing Process. *IBM J. Res. Dev.* **1961**, *5* (3), 183–191. https://doi.org/10.1147/rd.53.0183.

(67) performance, R. world; graphics, immersive graphics are at the heart of 11th G. I. C. P. with I. I. X. *Product Brief: 11th Gen Intel® Core™ Mobile Processors*. Intel. https://www.intel.com/content/www/us/en/products/docs/processors/core/11th-gen-core-mobile-processors-brief.html (accessed 2023-08-10).

(68) Gangnaik, A. S.; Georgiev, Y. M.; Holmes, J. D. New Generation Electron Beam Resists: A Review. *Chem. Mater.* **2017**, *29* (5), 1898–1917. https://doi.org/10.1021/acs.chemmater.6b03483.

(69) Vieu, C.; Carcenac, F.; Pépin, A.; Chen, Y.; Mejias, M.; Lebib, A.; Manin-Ferlazzo, L.; Couraud, L.; Launois, H. Electron Beam Lithography: Resolution Limits and Applications. *Appl. Surf. Sci.* **2000**, *164* (1–4), 111–117. https://doi.org/10.1016/s0169-4332(00)00352-4.

(70) Bunk, R.; Carlberg, P.; Månsson, A.; Nicholls, I. A.; Omling, P.; Sundberg, M.; Tågerud, S.; Montelius, L. Guiding Molecular Motors with Nano-Imprinted Structures. *Jpn. J. Appl. Phys.* **2005**, *44* (5A), 3337–3340. https://doi.org/10.1143/jjap.44.3337.

(71) Albet-Torres, N.; O'Mahony, J.; Charlton, C.; Balaz, M.; Lisboa, P.; Aastrup, T.; Månsson, A.; Nicholls, I. A. Mode of Heavy Meromyosin Adsorption and Motor Function Correlated with Surface Hydrophobicity and Charge. *Langmuir* **2007**, *23* (22), 11147–11156. https://doi.org/10.1021/la7008682.

(72) Lindberg, F. W.; Norrby, M.; Rahman, M. A.; Salhotra, A.; Takatsuki, H.; Jeppesen, S.; Linke, H.; Mansson, A. Controlled Surface Silanization for Actin-Myosin Based Nanodevices and Biocompatibility of New Polymer Resists. *Langmuir* **2018**, *34* (30), 8777–8784. https://doi.org/10.1021/acs.langmuir.8b01415.

(73) Sundberg, M.; Rosengren, J. P.; Bunk, R.; Lindahl, J.; Nicholls, I. A.; Tågerud, S.; Omling, P.; Montelius, L.; Månsson, A. Silanized Surfaces for in Vitro Studies of Actomyosin Function and Nanotechnology Applications. *Anal. Biochem.* **2003**, *323* (1), 127–138. https://doi.org/10.1016/j.ab.2003.07.022.

(74) Gardini, L.; Arbore, C.; Capitanio, M.; Pavone, F. S. A Protocol for Single Molecule Imaging and Tracking of Processive Myosin Motors. *MethodsX* **2019**, *6*, 1854–1862. https://doi.org/10.1016/j.mex.2019.08.011.

(75) Kron, S. J.; Toyoshima, Y. Y.; Uyeda, T. Q. P.; Spudich, J. A. Assays for Actin Sliding Movement over Myosin-Coated Surfaces. In *Methods in Enzymology*; Elsevier, 1991; pp 399–416. https://doi.org/10.1016/0076-6879(91)96035-p.

(76) Salhotra, A.; Zhu, J.; Surendiran, P.; Meinecke, C. R.; Lyttleton, R.; Ušaj, M.; Lindberg, F. W.; Norrby, M.; Linke, H.; Månsson, A. Prolonged Function and Optimization of Actomyosin Motility for Upscaled Network-Based Biocomputation. *New J. Phys.* **2021**, *23* (8), 085005. https://doi.org/10.1088/1367-2630/ac1809.

(77) Korten, T.; Diez, S.; Linke, H.; Nicolau, D. V.; Kugler, H. Design of Network-Based Biocomputation Circuits for the Exact Cover Problem. *New J. Phys.* **2021**, *23* (8), 085004.

(78) Zhu, J.; Salhotra, A.; Meinecke, C. R.; Surendiran, P.; Lyttleton, R.; Reuter, D.; Kugler, H.; Diez, S.; Månsson, A.; Linke, H.; Korten, T. Solving the 3-Satisfiability Problem Using Network-Based Biocomputation. *Adv. Intell. Syst.* **2022**, *4* (12), 2200202. https://doi.org/10.1002/aisy.202200202.

(79) Persson, M.; Albet-Torres, N.; Ionov, L.; Sundberg, M.; Höök, F.; Diez, S.; Månsson, A.; Balaz, M. Heavy Meromyosin Molecules Extending More Than 50 Nm above Adsorbing Electronegative Surfaces. *Langmuir* **2010**, *26* (12), 9927–9936. https://doi.org/10.1021/la100395a.

(80) Sundberg, M.; Bunk, R.; Albet-Torres, N.; Kvennefors, A.; Persson, F.; Montelius, L.; Nicholls, I. A.; Ghatnekar-Nilsson, S.; Omling, P.; Tågerud, S.; Månsson, A. Actin Filament Guidance on a Chip: Toward High-Throughput Assays and Lab-on-a-Chip Applications. *Langmuir* **2006**, *22* (17), 7286–7295. https://doi.org/10.1021/la060854i.

(81) Nitta, T.; Tanahashi, A.; Obara, Y.; Hirano, M.; Razumova, M.; Regnier, M.; Hess, H. Comparing Guiding Track Requirements for Myosin- and Kinesin-Powered Molecular Shuttles. *Nano Lett.* **2008**, *8* (8), 2305–2309. https://doi.org/10.1021/nl8010885.

(82) Månsson, A.; Bunk, R.; Sundberg, M.; Montelius, L. Self-Organization of Motor-Propelled Cytoskeletal Filaments at Topographically Defined Borders. *J. Biomed. Biotechnol.* **2012**, *2012*, 1–10. https://doi.org/10.1155/2012/647265.

(83) Bland, J. M.; Altman, D. G. Measuring Agreement in Method Comparison Studies. *Stat. Methods Med. Res.* **1999**, *8* (2), 135–160. https://doi.org/10.1177/096228029900800204.

(84) Giavarina, D. Understanding Bland Altman Analysis. *Biochem. Medica* **2015**, *25* (2), 141–151. https://doi.org/10.11613/BM.2015.015.

(85) Houbertz; Ruth; Steenhusen; Snke; Stiche; Thomas; Gerhar, S. Two-Photon Polymerization of Inorganic-Organic Hybrid Polymers as Scalable Technology Using Ultra-Short Laser Pulses. In *Coherence and Ultrashort Pulse Laser Emission*; InTech, 2010. https://doi.org/10.5772/13203.

(86) Finders, J.; Behringer, U. F.; Dietz, S.; Linke, H.; Lindberg, F.; Schulz, S. E.; Korten, T.; Domann, G.; Groß, M.; Heldt, G.; Meinecke, C.; Steenhusen, S.; Reuter, D. Approach to Combine Electron-Beam Lithography and Two-Photon Polymerization for Enhanced Nano-Channels in Network-Based Biocomputation Devices; 2018. https://doi.org/10.1117/12.2326598.

(87) Ovsianikov, A.; Schlie, S.; Ngezahayo, A.; Haverich, A.; Chichkov, B. N. Two-Photon Polymerization Technique for Microfabrication of CAD-Designed 3D Scaffolds from Commercially Available Photosensitive Materials. *J. Tissue Eng. Regen. Med.* **2007**, *1* (6), 443–449. https://doi.org/10.1002/term.57.

(88) Reuther, C.; Steenhusen, S.; Meinecke, C. R.; Surendiran, P.; Salhotra, A.; Lindberg, F. W.; Månsson, A.; Linke, H.; Diez, S. Molecular Motor-Driven Filament Transport across Three-Dimensional, Polymeric Micro-Junctions. *New J. Phys.* **2021**, *23* (12), 125002. https://doi.org/10.1088/1367-2630/ac39b4.

(89) Lindberg, F. W.; Korten, T.; Löfstrand, A.; Rahman, M. A.; Graczyk, M.; Månsson, A.; Linke, H.; Maximov, I. Design and Development of Nanoimprint-Enabled Structures for Molecular Motor Devices. *Mater. Res. Express* **2018**, *6* (2). https://doi.org/10.1088/2053-1591/aaed10.

(90) Fiorini, G. S.; Chiu, D. T. Disposable Microfluidic Devices: Fabrication, Function, and Application. *BioTechniques* **2005**, *38* (3), 429–446. https://doi.org/10.2144/05383rv02.

(91) Thorsen, T. Microfluidic Large-Scale Integration. *Science* **2002**, *298* (5593), 580–584. https://doi.org/10.1126/science.1076996.

(92) Craighead, H. G. Nanoelectromechanical Systems. *Science* **2000**, *290* (5496), 1532–1535. https://doi.org/10.1126/science.290.5496.1532.

(93) Esmek, F. M.; Bayat, P.; Pérez-Willard, F.; Volkenandt, T.; Blick, R. H.; Fernandez-Cuesta, I. Sculpturing Wafer-Scale Nanofluidic Devices for DNA Single Molecule Analysis. *Nanoscale* **2019**, *11* (28), 13620–13631. https://doi.org/10.1039/c9nr02979f.

(94) Fernandez-Cuesta, I.; West, M. M.; Montinaro, E.; Schwartzberg, A.; Cabrini, S. A Nanochannel through a Plasmonic Antenna Gap: An Integrated Device for Single Particle Counting. *Lab. Chip* **2019**, *19* (14), 2394–2403. https://doi.org/10.1039/c9lc00186g.

(95) Marie, R.; Pedersen, J. N.; Bauer, D. L. V.; Rasmussen, K. H.; Yusuf, M.; Volpi, E.; Flyvbjerg, H.; Kristensen, A.; Mir, K. U. Integrated View of Genome Structure and Sequence of a Single DNA Molecule in a Nanofluidic Device. *Proc. Natl. Acad. Sci.* **2013**, *110* (13), 4893–4898. https://doi.org/10.1073/pnas.1214570110.

(96) Unksov, I. N.; Korosec, C. S.; Surendiran, P.; Verardo, D.; Lyttleton, R.; Forde, N. R.; Linke, H. Through the Eyes of Creators: Observing Artificial Molecular Motors. *ACS Nanosci. Au* **2022**, *2* (3), 140–159. https://doi.org/10.1021/acsnanoscienceau.1c00041.

(97) Kassem, S.; Van Leeuwen, T.; Lubbe, A. S.; Wilson, M. R.; Feringa, B. L.; Leigh, D. A. Artificial Molecular Motors. *Chem. Soc. Rev.* **2017**, *46* (9), 2592–2621. https://doi.org/10.1039/c7cs00245a.

(98) Korosec, C. S.; Zuckermann, M. J.; Forde, N. R. Dimensionality-Dependent Crossover in Motility of Polyvalent Burnt-Bridges Ratchets. *Phys. Rev. E* **2018**, *98* (3). https://doi.org/10.1103/physreve.98.032114.

(99) Salhotra, A.; Rahman, M. A.; Ruijgrok, P. V.; Meinecke, C. R.; Ušaj, M.; Zemsky, S.; Lindberg, F. W.; Surendiran, P.; Lyttleton, R. W.; Linke, H.; Korten, T.; Bryant, Z.; Månsson, A. Exploitation of Engineered Light-Switchable Myosin XI for Nanotechnological Applications. *ACS Nano* **2023**. https://doi.org/10.1021/acsnano.3c05137.

The parallel computing approach of 'network-based biocomputation' involves using biomolecular machines to navigate through a nanofabricated network of channels, representing a mathematical algorithm, to solve problems. This thesis investigates various aspects of scaling and enhancing the performance of this approach, such as developing optimized nanodevices, solving multiple problems, and addressing error rates.

Printed by Media-Tryck, Lund 2023 NORDIC SWAN ECOLABEL 3041 0903

LUND UNIVERSITY

Faculty of Engineering
Department of Physics
Solid State Physics

ISBN 978-91-8039-811-4